Nano Research

ISSN 1998-0124 CN 11-5974/O4
https://doi.org/10.26599/NR.2026.94908703

Research Article

Interfacial micro-capacitor engineering in CF/hyperbranched polyamide/RGO composites for efficient microwave absorption

Boshi Gao[1,2,3], Yuefeng Yan[1,2,3](✉), Xin Huang[4], Jingzhe Hong[1,2,3], Tao Chen[1,2,3], Naiyu Jiang[5](✉), Haitang Yang[4](✉), Dechang Jia[1,2,3], Yu Zhou[1,2,3], Xiaoxiao Huang[1,2,3](✉)

[1] MIIT Key Laboratory of Advanced Structural-Functional Integration Materials & Green, Manufacturing Technology, Harbin Institute of Technology, Harbin 150001, China

[2] School of Materials Science and Engineering, Harbin Institute of Technology, Harbin 150001, China

[3] National Key Laboratory of Precision Welding & Joining of Materials and Structures, Harbin Institute of Technology, Harbin 150001, China

[4] AVIC Chengdu Aircraft Industrial (Group) CO., LTD., Chengdu 610092, China

[5] Institute of Composite Materials and Structures, Harbin Institute of Technology, Harbin 150001, China

Nano Res., **Just Accepted Manuscript** • https://doi.org/10.26599/NR.2026.94908703
https://www.sciopen.com/journal/1998-0124 on Apr. 1, 2026

Table of Contents

Boshi Gao[1,2,3], Yuefeng Yan[1,2,3*], Xin Huang[4], Jingzhe Hong[1,2,3], Tao Chen[1,2,3], Naiyu Jiang[5*], Haitang Yang[4*], Dechang Jia[1,2,3], Yu Zhou[1,2,3] and Xiaoxiao Huang[1,2,3*]

RC microcircuits enable broadband absorption under ultrathin conditions.

An RC microcircuit array is constructed within CF@HP@RGO composites via a heterogeneous conductive-dielectric-conductive interface. The evolution of sp^2 domains regulates defect density and interfacial polarization, while the nanoscale dielectric layer induces strong localized electric fields. These synergistic effects enable optimized impedance matching and enhanced dielectric relaxation, resulting in superior microwave absorption under ultrathin thickness and low filler loading.

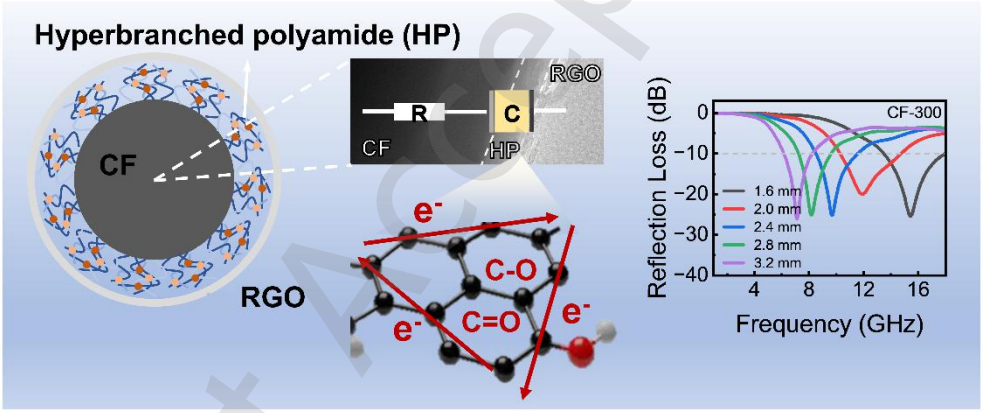

Research Article

Interfacial micro-capacitor engineering in CF/hyperbranched polyamide/RGO composites for efficient microwave absorption

Boshi Gao[1,2,3], Yuefeng Yan[1,2,3*], Xin Huang[4], Jingzhe Hong[1,2,3], Tao Chen[1,2,3], Naiyu Jiang[5*], Haitang Yang[4*], Dechang Jia[1,2,3], Yu Zhou[1,2,3], and Xiaoxiao Huang[1,2,3*]

1. MIIT Key Laboratory of Advanced Structural-Functional Integration Materials & Green, Manufacturing Technology, Harbin Institute of Technology, Harbin 150001, China

2. School of Materials Science and Engineering, Harbin Institute of Technology, Harbin 150001, China

3. National Key Laboratory of Precision Welding & Joining of Materials and Structures, Harbin Institute of Technology, Harbin 150001, China

4. AVIC Chengdu Aircraft Industrial (Group) CO., LTD., Chengdu 610092, China

5. Institute of Composite Materials and Structures, Harbin Institute of Technology, Harbin 150001, China

Received: 18 March 2026; **Revised:** 30 March 2026; **Accepted:** 1 April 2026

*Address correspondence to Xiaoxiao Huang, swliza@hit.edu.cn; Yuefeng Yan, 22B909026@stu.hit.edu.cn; Haitang Yang, 371136039@qq.com; Naiyu Jiang, jiangnaiyu0904@163.com

Cite this article: *Nano Research*, 2026, 19, 94908703 https://doi.org/10.26599/NR.2026.94908703

Abstract

Developing lightweight electromagnetic wave absorbers with low filler loading remains challenging. However, carbon materials rarely achieve strong attenuation capability, wide absorption bandwidth, lightweight and thin thickness simultaneously. Herein, a carbon fiber-hyperbranched polyamide-reduced graphene oxide (CF-HP-RGO) interfacial micro-capacitor architecture was rationally constructed through thermal reduction. The incorporation of HP and RGO introduces dual heterogeneous interfaces between carbon fibers and RGO layers, while forming CF-HP-RGO micro-capacitor units that act as dominant polarization centers. Under alternating electromagnetic fields, these micro-capacitor interfaces generate pronounced charge accumulation and interfacial polarization, thereby strengthening dielectric relaxation and polarization loss. Meanwhile, the interconnected RGO network establishes efficient electron-transport pathways, producing additional conductive loss. In addition, the multilayer hierarchical interface enhances multiple scattering, effectively extending electromagnetic propagation paths and improving attenuation efficiency. As a result, the optimized composite delivers a maximum effective absorption bandwidth of 5.24 GHz in the Ku band at an ultrathin thickness of 1.6 mm with a filler loading of only 5 wt.%. This work highlights micro-capacitor-dominated interfacial engineering as a promising route toward lightweight and high-performance electromagnetic wave absorption in carbon materials.

Keywords: interfacial engineering, micro-capacitor, electromagnetic wave absorber, interfacial polarization

1. Introduction

With the rapid development of radar detection and satellite communication technologies, electromagnetic radiation has become an increasingly serious issue affecting precision electronics, human health, and information security [1]. Therefore, the development of lightweight electromagnetic wave absorbing materials (EAMs) featuring low filler loading, broad effective absorption bandwidth (EAB), and high attenuation efficiency has attracted extensive research interest. Carbon-based materials are regarded as promising candidates for EAMs due to their low density, high chemical stability, excellent electrical conductivity, and favorable dielectric loss properties [2]. Representative materials such as carbon fibers, graphene, porous carbon foams, hollow carbon spheres, and carbon nanotubes demonstrate significant potential in lightweight electromagnetic protection applications. The electromagnetic attenuation capability of carbon materials mainly originates from conductive loss, dipolar polarization, and multiple scattering mechanisms [3]. Importantly, their complex permittivity and attenuation behavior can be effectively tuned through rational structural engineering [4, 5]. To this end, numerous studies have explored strategies such as morphology regulation (e.g., flower-like, rod-like, and spherical structures), heteroatom doping (e.g., Fe and N doping), and hierarchical architecture design, including interfacial engineering and gradient porous structures, to enhance microwave absorption performance [6].

Carbon fibers are considered promising candidates for EAMs due to their high mechanical strength, large aspect ratio, and excellent electrical loss characteristics. Compared with carbon spheres or porous carbon frameworks, carbon fibers can more efficiently establish conductive networks within polymer matrices such as paraffin, thereby enhancing dielectric loss behavior [7]. Nevertheless, the inherently high permittivity of carbon fibers often leads to severe impedance mismatch, resulting in strong reflection of incident electromagnetic waves at the material surface rather than effective absorption within the interior [8]. Consequently, the microwave attenuation

capability of pristine carbon fibers remains limited [9]. To overcome this drawback, extensive efforts have focused on constructing heterogeneous architectures by integrating carbon fibers with dielectric materials, magnetic metals, or metal oxides to optimize impedance matching [10]. For instance, decorating carbon fibers with magnetic nanoparticles can introduce magnetic loss mechanisms and achieve synergistic dielectric-magnetic attenuation [11]. Alternatively, coating dielectric layers such as SiO_2 , TiO_2 , or ZnO on carbon fiber surfaces can improve impedance matching through polarization losses generated at abundant heterogeneous interfaces [12, 13]. Among these strategies, graphene coatings have attracted particular interest owing to their ultrahigh specific surface area and excellent electrical conductivity [14]. The efficient electron-transport pathways provided by graphene can significantly enhance dielectric loss, while its two-dimensional structure facilitates the construction of complex interfacial architectures.

Nevertheless, the development of high-performance carbon-fiber-based EAMs still faces several intrinsic challenges [15]. First, most reported carbon fiber systems primarily rely on conductive loss for electromagnetic attenuation, whereas the role of interfacial polarization in dielectric loss has received comparatively limited attention [16, 17]. Second, the extremely high conductivity of carbon fibers often results in severe impedance mismatch, making it difficult to simultaneously optimize dielectric loss and impedance matching [18]. Third, many high-performance absorber systems depend on complex multi-component architectures or high filler loading, which inevitably increase density and fabrication cost [19]. For lightweight dielectric absorbers, pure carbon-based systems remain particularly attractive. In this regard, engineering heterogeneous interfaces has been recognized as an effective approach to enhance polarization loss and electromagnetic attenuation [20]. Interfaces with distinct dielectric properties can induce charge accumulation and polarization under alternating electromagnetic fields, thereby facilitating dielectric relaxation. Notably, interfaces between conductive carbon frameworks and dielectric materials can behave

as localized charge-storage units, enabling repeated polarization under alternating electromagnetic waves [21]. Such heterogeneous interfaces operate in a manner analogous to micro capacitors, where opposite charges accumulate across the interface under electromagnetic excitation [22, 24]. These interfacial micro capacitors cooperate with micro-resistors formed by conductive carbon networks, repeatedly undergoing charge storage, release, and dissipation, thereby generating strong interfacial polarization and dielectric loss. However, constructing stable and uniformly distributed micro capacitor interfaces on lightweight carbon fiber surfaces remains largely unexplored, and requires the rational integration of conductive networks, dielectric components, and hierarchical interface structures.

Hyperbranched polyamide (HP) has attracted considerable attention as a dielectric component due to its abundant polar functional groups and highly branched molecular architecture. The numerous terminal groups can serve as polarization centers under electromagnetic excitation, while the carbonyl groups in HP can form hydrogen bonds with both carbon fibers and graphene sheets, enabling the construction of stable hierarchical interfaces. Reduced graphene oxide (RGO), a two-dimensional conductive carbon material, provides efficient electron transport pathways and facilitates the formation of conductive networks. Meanwhile, its layered structure introduces abundant interfacial sites and structural defects, which further enhance polarization effects. Herein, a hierarchical carbon fiber-HP-reduced graphene oxide (CF-HP-RGO) architecture was rationally constructed via a controlled thermal reduction strategy. The reduction degree of graphene oxide (GO) was tuned by adjusting the reduction temperature. Within this structure, carbon fibers act as the main conductive framework and serve as resistive elements in the equivalent microcircuit, while HP functions as the dielectric layer of the micro capacitor. The outer RGO sheets form a continuous conductive layer, which constructs interfacial micro capacitor units with the carbon fiber surface and dielectric layer, thereby inducing pronounced charge accumulation and interfacial polarization. As a result, the

synergistic effects of micro capacitor polarization, conductive loss, and structural multiple scattering enable the optimized composite to achieve excellent microwave absorption performance in the Ku band. These findings provide a new strategy for constructing micro capacitor-dominated dielectric attenuation architectures in pure carbon systems and offer guidance for designing lightweight and high-efficiency EAMs.

2. Experimental

2.1. Materials

carbon fiber T700 (Toray Industries, Inc. in Japan), Acetone, N-Aminoethylpiperazine (AEP), N, N'-Bis(acrylonitrile-2,4-diyl) amine (MBA), Flattened Sulfuric Acid (H_2SO_4), phosphoric acid (H_3PO_4), Graphite, Potassium permanganate ($KMnO_4$), Hydrogen peroxide (H_2O_2) (Aladdin Reagents Co., Ltd. and are of analytical grade).

2.2. Preparation of GO

GO was prepared following a modified Hummers' method. Concentrated sulfuric acid (180 mL) was added slowly to phosphoric acid (20 mL) and mixed thoroughly. Graphite powder (1.5 g) was then added, and the mixture was stirred for 10 min. While maintaining the temperature at 50 °C, potassium permanganate (9 g) was added slowly over several minutes, ensuring the reaction temperature remained within 49-51 °C. After addition, the mixture was kept at 50 °C for 6 h. Subsequently, hydrogen peroxide (130 mL) was added dropwise, changing the solution color from black to bright yellow. The mixture was then maintained at 50 °C for 3 h, cooled to room temperature, and washed by centrifugation at 9000 rpm for 5 min per cycle. The solid product was dialyzed in deionized water for 7 days, yielding a 5 mg mL^{-1} GO solution.

2.3. Preparation of HP

AEP (20.16 g, 0.156 mol) was dissolved in 300 mL deionized water, followed by the addition of MBA (18.5 g, 0.12 mol). The solution was stirred at 60 °C for 24 h, then concentrated by rotary evaporation at 90 °C to obtain a viscous orange-yellow colloid. The product was washed by triple precipitation with acetone and water, and vacuum-dried at 60 °C for 12 h to yield HP.

2.4. Preparation of CF-300

Carbon fibers were boiled in acetone at 80 °C for 48 h to remove the surface protective layer, followed by drying at 80 °C for 4 h. A 10 mg mL^{-1} solution of HP was prepared and used to modify the fibers. The degummed carbon fibers were immersed in the HP-2 solution at 30 °C for 12 h, then dried at 100 °C for 2 h to obtain HP-coated carbon fibers. For electroplating, the HP-coated carbon fiber was connected to the cathode, while a graphite plate served as the anode, with a 3 cm electrode spacing. The GO solution used had a concentration of 0.3 mg mL^{-1} and a pH of 10. Electrodeposition was performed at 20 V for 5 min, followed by drying at 80 °C for 6 h to yield CF@HP@GO. CF@HP@GO composites were thermally reduced under an argon atmosphere at 200 °C, 300 °C, and 400 °C. The resulting carbon fiber samples were denoted as CF-200, CF-300, and CF-400, respectively. To further investigate the chemical states of the HP coating and GO layers under different thermal reduction conditions, pure HP and GO samples were simultaneously subjected to thermal reduction in the same chamber. The resulting products were designated as HP-200, HP-300, and HP-400, as well as RGO-200, RGO-300, and RGO-400, respectively.

2.5. Characterization and measurements

This section was described in the Supporting Information.

3. Results and discussion

3.1 Structural design and microstructure characterization of CF/HP/RGO interface

To construct the designed interfacial micro capacitor architecture, carbon fibers were

first impregnated in a HP solution to form a uniform dielectric coating. Subsequently, GO layers were deposited onto the carbon fiber surface via electrodeposition, forming a hierarchical CF-HP-GO structure. After electrodeposition, carbon fibers were thermally reduced under a protective atmosphere at 200 °C, 300 °C, and 400 °C, resulting in reduced graphene oxide (RGO) coatings with different reduction degrees and corresponding interfacial micro capacitor layers with distinct matching characteristics (**Fig. 1**a). The carbon fibers coated with HP-GO coating and the reduced samples are designated as CF-0, CF-200, CF-300 and CF-400, respectively. Inspired by classical capacitor configurations, a micro capacitor-dominated interfacial structure was constructed on the conductive carbon fiber surface. Transmission electron microscopy (TEM) images of the interface, together with schematic illustrations of the micro capacitor architecture, reveal the equivalent microcircuit configuration of the system (Fig. 1b). By dividing the carbon fiber cross-section into infinitesimal sector elements, the structure can be equivalently modeled as a distributed resistor-parallel-plate capacitor (RC) circuit. In this equivalent circuit, the conductive carbon fiber acts as a micro-resistor, while the HP dielectric layer and outer RGO sheet function as the capacitor components. This RC equivalent model is consistent with the interfacial structure observed in TEM images [25]. When electromagnetic waves are incident on the carbon fiber surface, the resulting electric field distribution can be described by Equation (1):

$$E(t) = E_0 e^{i\omega t} \quad (1)$$

where $E(t)$ is the instantaneous electric field intensity, E_0 is the electric field amplitude, i is the imaginary unit, and ω is the angular frequency. When subjected to an alternating electric field, charge carriers accumulate at the heterogeneous interfaces constructed by conductive carbon fibers, dielectric HP layers, and outer reduced graphene oxide sheets. These interfaces behave analogously to micro capacitor units, in which the conductive carbon fiber acts as a micro-resistor and the CF-HP-RGO interfacial layer functions as the capacitor component. Accordingly, the dynamic

charging and discharging processes of these interfacial micro capacitors can be described using the classical RC circuit as shown by Equation (2):

$$\frac{dQ}{dt} + \frac{Q}{RC} = \frac{V(t)}{R} \tag{2}$$

where Q is the accumulated interfacial charge, $R$is the equivalent resistance associated with the conductive carbon fiber network, C is the equivalent capacitance of the interfacial dielectric layer, and $V(t)$ is the applied potential induced by the incident electromagnetic field. The characteristic response time of the micro capacitor interface is governed by the RC time constant:

$$\tau = RC \tag{3}$$

where τ represents the relaxation time associated with the charge accumulation and dissipation processes at the heterogeneous interface. When the frequency of the incident electromagnetic field approaches the reciprocal of the relaxation time ($\omega\tau \approx 1$), the interfacial polarization reaches its maximum intensity. From the perspective of dielectric relaxation theory, the complex permittivity of the system can be expressed according to the Debye relaxation model:

$$\varepsilon^*(\omega) = \varepsilon' - i\varepsilon'' = \varepsilon_\infty + \frac{\varepsilon_s - \varepsilon_\infty}{1 + i\omega\tau} \tag{4}$$

where $\varepsilon^*(\omega)$ is the complex permittivity, ε' and ε'' represent the real and imaginary parts of permittivity, respectively, ε_s is the static permittivity, ε_∞ is the high-frequency permittivity limit, and τ is the dielectric relaxation time. Therefore, the interfacial micro capacitor architecture constructed in the CF-HP-RGO system forms a distributed RC microcircuit network. Under alternating electromagnetic excitation, these micro capacitors repeatedly undergo charge accumulation, storage, and release processes, generating strong interfacial polarization and dielectric relaxation. This mechanism significantly enhances dielectric loss and contributes to efficient electromagnetic wave attenuation.

To further verify the electromagnetic attenuation mechanism governed by the interfacial micro capacitor architecture, finite-element simulations were conducted using COMSOL Multiphysics to investigate the spatial distribution of electromagnetic loss within the composite. The simulation results reveal that the attenuation capability of the micro capacitor interface is strongly dependent on the reduction degree of RGO. For the CF-200 interface, the loss field is predominantly confined to the carbon fiber interior, suggesting insufficient activation of the interfacial micro capacitor structure. In contrast, the CF-300 interface exhibits pronounced loss regions simultaneously within the RGO sheets and the carbon fiber core, accompanied by significantly intensified energy dissipation at the micro capacitor interface. When the reduction temperature increases to 400 °C, strong attenuation becomes localized near the RGO layers, while the internal loss within the carbon fiber decreases, indicating an imbalance in the conductive-capacitive coupling of the interfacial structure. These results suggest that at 300 °C the carbon fiber surface and RGO sheets achieve optimal electrical matching and function as effective capacitive electrodes within the interfacial RC microcircuit network. Therefore, CF-300 is expected to exhibit a markedly enhanced the imagine part of complex permittivity (ε″), reflecting superior electromagnetic energy dissipation capability. The multi-interface polarization processes arising from this distributed RC microcircuit network are typically manifested as semicircular arcs in Cole-Cole plots, indicating enhanced dielectric relaxation behavior and improved microwave attenuation performance.

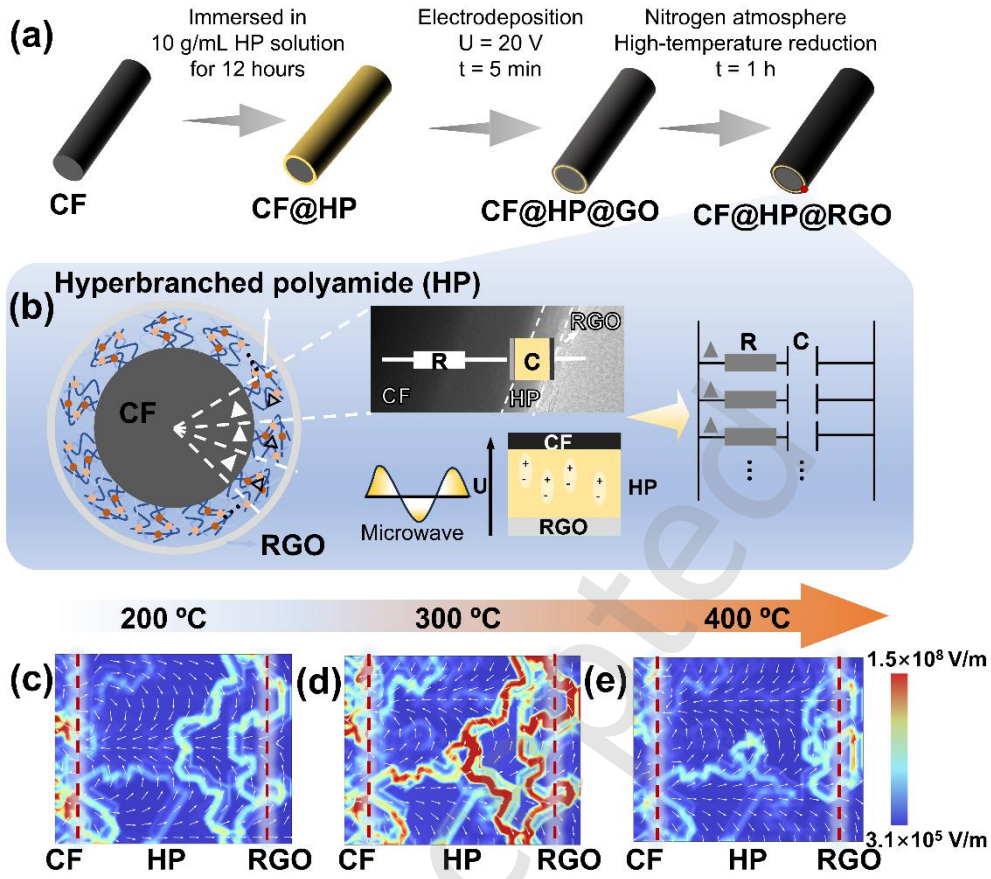

Figure. 1 Design and Fabrication of RC Microcircuit Structure. (a) Schematic diagram of the preparation process of CF@HP@RGO. (b) Analysis of RC Microcircuit Structure. RC Microcircuit Structural Loss Field Simulation of (c) CF-200, (d) CF-300 and (e) CF-400.

The phase evolution of GO during thermal reduction was investigated by XRD (**Fig. 2**a). GO exhibits a sharp diffraction peak at approximately 2θ ≈ 12°, corresponding to the (002) plane of GO. After thermal treatment, this peak disappears for all reduced samples, indicating the successful transformation of GO into reduced graphene oxide (RGO) at reduction temperatures between 200 and 400 °C. Additionally, a broad diffraction peak centered near 2θ ≈ 23° emerges in all reduced samples, which is a characteristic feature of RGO structures. With increasing reduction temperature, the peak at 23° becomes progressively narrower, suggesting a higher reduction degree and improved structural ordering of the graphene layers. Raman spectroscopy was

further conducted to evaluate structural defects in GO and RGO (Fig. 2b). Both GO and RGO display two characteristic bands located at approximately 1350 cm^{-1} (D band) and 1580 cm^{-1} (G band). The D band originates from structural disorder, while the G band corresponds to the in-plane vibration of sp^2 carbon networks. The I_D/I_G ratio is commonly used to evaluate defect density, where larger values indicate increased structural disorder. The I_D/I_G ratios of GO, RGO-200, RGO-300, and RGO-400 are 0.848, 0.876, 0.885, and 0.878, respectively, suggesting a slight increase in defect density after thermal reduction. FTIR spectroscopy was employed to analyze the evolution of oxygen-containing functional groups (Fig. 2c). GO shows characteristic absorption peaks corresponding to C-O-C (1264 cm^{-1}), adsorbed water (1634 cm^{-1}), C=O (1720 cm^{-1}), and -OH stretching (3430 cm^{-1}). As the reduction temperature increases, the -OH peak gradually weakens and the intensity of oxygen-containing functional groups decreases significantly, indicating the progressive removal of oxygen functional groups during the reduction process.

The chemical states of surface elements and the phase composition of the micro capacitor interface on the carbon fibers were investigated by X-ray photoelectron spectroscopy (XPS). As shown in Fig. 2d, the survey spectrum clearly reveals the presence of C, O, and N elements. The relatively weak N signal originates from the structural configuration of the interface, where the carbon fiber surface is coated with an approximately 80 nm thick HP layer that is further covered by GO or RGO sheets, thereby attenuating the nitrogen signal detected from the outer surface. The high-resolution C1s spectrum (Fig. 2e) was used to analyze the chemical bonding states of carbon. Three characteristic peaks located at 284.8 eV, 285.9 eV, and 289.6 eV can be assigned to C-C, C-O, and C=O bonds, respectively. With increasing reduction temperature, the reduction degree of GO gradually increases, accompanied by a noticeable decrease in both the intensity and width of oxygen-containing functional group peaks. In CF-400, the C=O-related peak becomes nearly undetectable, indicating extensive removal of oxygen functional groups during

thermal reduction. This may reduce the number of defect-related polarization sites within the graphene layer. The high-resolution N1s spectrum provides further insight into the chemical bonding configuration of HP on the carbon fiber surface. Peaks located at 400.39 eV, 400.5 eV, and 401.37 eV are attributed to N-H, N-C, and N-O bonding environments, respectively. As the reduction temperature increases, the N-O component gradually decreases, suggesting partial modification of nitrogen-related functional groups during thermal treatment. However, due to the relatively weak nitrogen signal detected from the surface, FTIR spectroscopy and additional XPS elemental analysis were performed on pure HP samples to further verify its chemical stability under different reduction temperatures.

FTIR spectroscopy was further conducted to evaluate the chemical stability of the HP polymer coating after thermal reduction (Fig. S3). As the reduction temperature increases, the intensities of the characteristic absorption peaks of HP gradually decrease, indicating partial modification of functional groups during thermal treatment. Nevertheless, the main characteristic peaks remain clearly observable, suggesting that the fundamental chemical structure of HP is largely retained. The peaks located at 1232, 1537, 1640, and 3305 cm^{-1} correspond to amide III, amide II, amide I, and N-H stretching vibrations, respectively, which are characteristic functional groups of HP. The FTIR spectra of samples treated at different temperatures display consistent characteristic absorption peaks corresponding to amide functional groups, suggesting that the chemical framework of the HP coating remains largely preserved during the thermal reduction process. The thermal stability of the HP polymer layer was further evaluated by XPS spectroscopy. Distinct C-N and C=O bonding features are observed in the XPS spectra, and their binding energies exhibit negligible changes with increasing treatment temperature (Fig. S4). Because C-N and C=O bonds are the most representative chemical bonding structures of HP, these results provide additional evidence for the stable retention of the HP layer on the carbon fiber surface. HP-400 exhibits nearly identical macroscopic morphology to

pristine HP (Fig. S5, 6). Although a small amount of adsorbed water may be released during thermal reduction, the fundamental chemical structure remains essentially unchanged, ensuring the structural stability of the dielectric layer within the CF-HP-RGO micro capacitor interface. Comparative analysis reveals that the O/C atomic ratio gradually decreases with increasing reduction temperature, indicating the progressive removal of oxygen-containing functional groups and the partial restoration of the sp^2 carbon framework in graphene (Fig. 2g). The sp^2 carbon refers to graphitic or conjugated carbon regions with a planar bonding configuration, which are primarily associated with C=C bonds in graphene-like structures. The content of sp^2 carbon is influenced by multiple factors, including interfacial interactions, thermally induced defect formation, and the evolution of heteroatom incorporation and bonding. Meanwhile, quantitative analysis based on Equation S1 shows that the sp^2 content exhibits a non-monotonic trend, initially increasing and subsequently decreasing with increasing reduction temperature. At relatively low reduction temperatures, the elimination of epoxy functional groups leads to the formation of numerous small sp^2 domains, which introduce abundant defects and domain boundaries into the graphene lattice, thereby increasing the sp^2 content. As the reduction temperature further increases, the graphene structure undergoes partial graphitic reconstruction, promoting the growth and coalescence of sp^2 domains, accompanied by the repair of structural defects, which results in a decrease in sp^2 content. This optimized defect configuration at 300 °C provides the most favorable condition for interfacial polarization and dielectric relaxation, thereby contributing to the superior microwave absorption performance of CF-300.

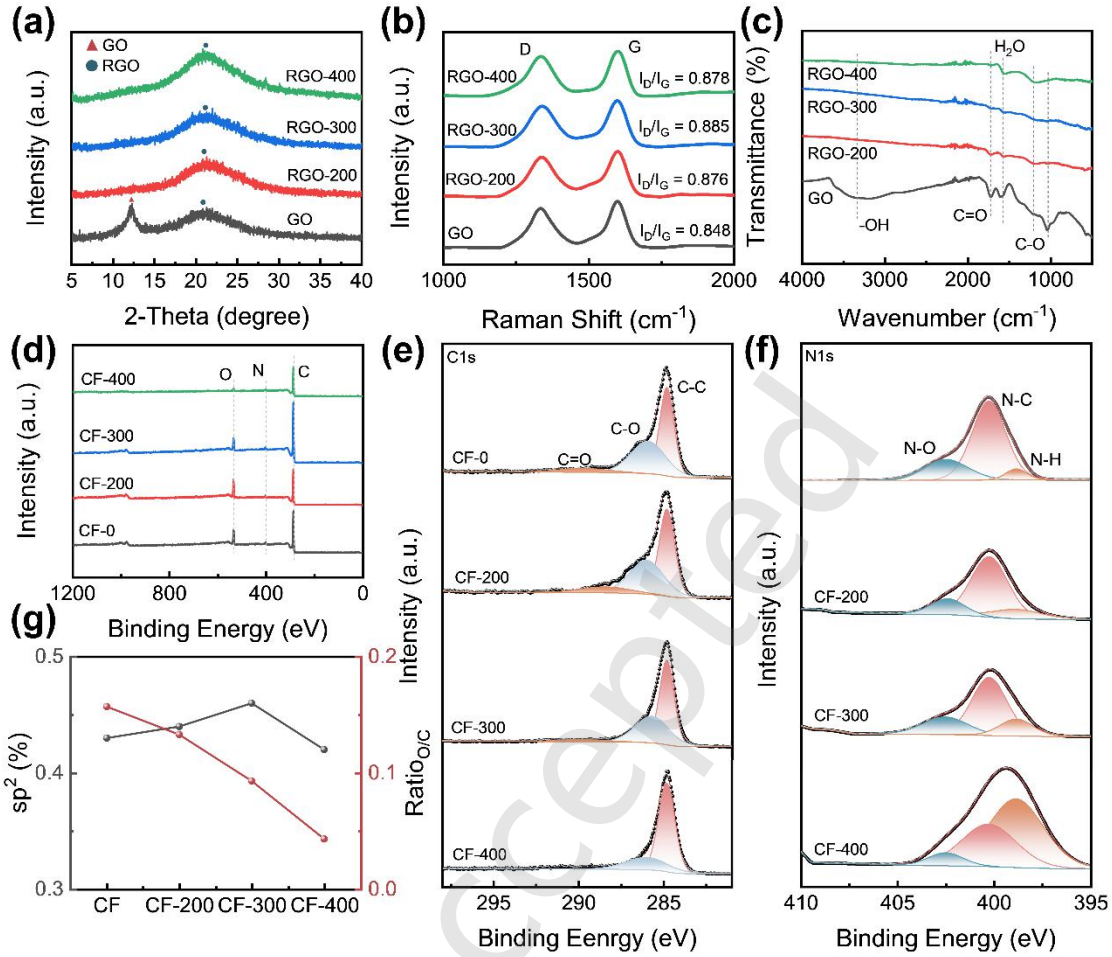

Figure. 2 Characterization of RGO and CF structural components. (a) XRD pattern, (b) Raman spectrum, and (c) infrared spectrum of GO~RGO-400 sample. (d) XPS spectrum, (e) C spectrum, and (f) N spectrum of CF-0~CF-400. (g) Defect and functional group comparison diagram of CF-0~CF-400.

The microstructure of the carbon fibers was investigated by scanning electron microscopy (SEM) combined with energy dispersive spectroscopy (EDS). As shown in Fig. S7 and S8, the pristine carbon fibers exhibit a smooth and clean surface with a well-defined cylindrical morphology. After the introduction of the HP polymer coating and subsequent deposition of GO, the surface morphology changes significantly. The fiber surface becomes noticeably rough, and a continuous coating layer uniformly covers the entire fiber surface (**Fig. 3**a1-a2), indicating successful deposition of both HP and GO. Importantly, after thermal reduction at 200-400 °C, the

HP-RGO coating remains intact without visible cracks or structural damage (Fig. 3b1-d1, b2-d2), demonstrating excellent structural stability of the interfacial coating during the reduction process. To further evaluate the spatial uniformity of the coating, EDS elemental mapping was performed. The elemental distribution maps reveal a uniform distribution of oxygen and nitrogen elements across the fiber surface (Fig. 3a3-d3, a4-d4). The oxygen signal mainly originates from oxidized graphene and oxygen-containing groups in HP, while nitrogen is primarily associated with the amide groups of the HP polymer. The homogeneous nitrogen distribution provides strong evidence for the successful and uniform incorporation of the polymer coating. Moreover, the uniform elemental distribution suggests minimal graphene sheet aggregation and negligible organic clustering during the GO deposition process. Such a uniform HP-RGO coating provides a well-defined heterogeneous interface on the carbon fiber surface, which is crucial for constructing the interfacial micro capacitor structure and enhancing interfacial polarization during electromagnetic wave attenuation. Transmission electron microscopy (TEM) images further reveal the detailed interfacial structure of the CF-HP-RGO system. As shown in Fig. 3e, a distinct intermediate layer with irregular contrast is clearly observed between the carbon fiber surface and the outer GO nanosheets. This intermediate layer corresponds to the HP polymer coating, forming a well-defined interfacial structure with clear boundaries. The relatively uniform thickness of this intermediate layer indicates that HP forms a continuous and homogeneous coating on the carbon fiber surface. Such a CF-HP-RGO interfacial configuration can function as a micro capacitive unit, which promotes interfacial polarization under alternating electromagnetic fields and enhances electromagnetic wave attenuation. Furthermore, with increasing reduction temperature and the thickness of the HP layer between the carbon fiber surface and the reduced graphene oxide layer remain essentially unchanged (Fig. 3f-h). This suggests that the reduction degree of RGO can be treated as the primary variable within the CF-HP-RGO micro capacitor structure. Combined

SEM, EDS, and TEM analyses confirm the successful formation of a stable interfacial coating on the carbon fiber surface, demonstrating the construction of a heterogeneous carbon fiber-polymer-carbon architecture. This unique hierarchical interface is expected to introduce abundant polarization sites and promote the formation of micro capacitor array structures, thereby significantly enhancing electromagnetic wave attenuation capability. Such a micro capacitor-dominated interfacial architecture enables repeated charge accumulation and release under alternating electromagnetic fields, thereby significantly enhancing interfacial polarization and dielectric loss.

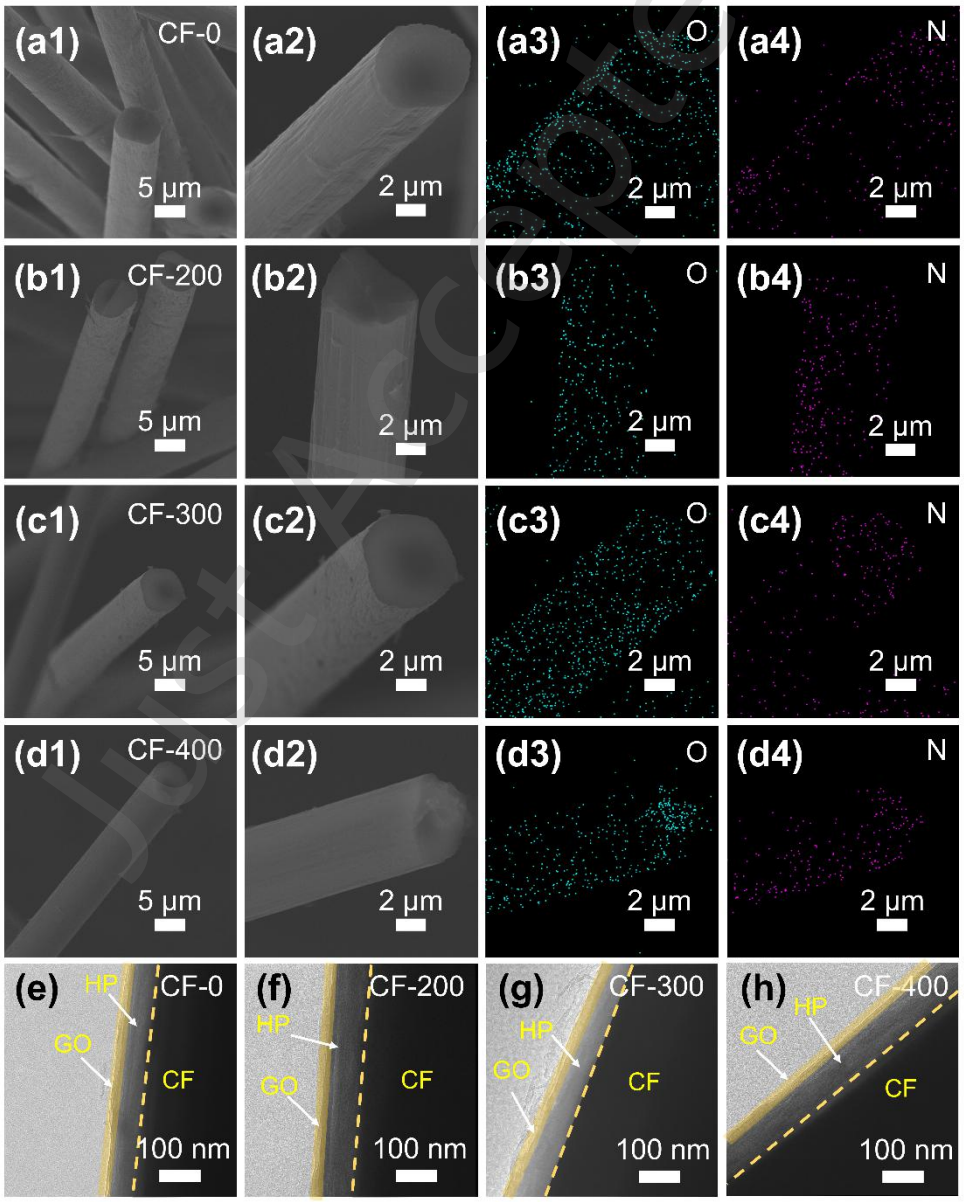

Figure. 3 Interface morphology and elemental characterization. SEM images and elemental energy dispersive spectroscopy (EDS) patterns of (a) CF-0, (b) CF-200, (c) CF-300, and (d) CF-400. Micro capacitive interface TEM images of (e) CF-0, (f) CF-200, (g) CF-300, and (h) CF-400.

3.2 Dielectric properties and microwave absorption performance

The electromagnetic parameters of CF@HP@RGO composites were measured in the 1-18 GHz frequency range to evaluate their microwave absorption behavior. As shown in **Fig. 4**a, both the real (ε′) and imaginary (ε″) components of the complex permittivity decrease with increasing frequency, exhibiting typical dielectric dispersion behavior. With increasing reduction temperature, the degree of RGO reduction increases, resulting in an initial increase followed by a decrease in both ε′ and ε″. Among the samples, CF-300 exhibits a significantly higher ε″ value, indicating enhanced dielectric loss capability. This improvement originates from the RC micro capacitor array formed by the conductive carbon fiber framework and the dielectric HP layer, which enables repeated charge accumulation and release at heterogeneous interfaces under alternating electromagnetic fields, thereby significantly enhancing interfacial polarization and dielectric loss. The imaginary part of the complex permittivity for EAMs can be obtained using Equation (5):

$$\varepsilon'' = \frac{(\varepsilon_s - \varepsilon_\infty)\omega\tau}{1+(\omega\tau)^2} \quad (5)$$

where ε_s denotes the static dielectric constant, ε_∞ represents the dielectric constant at the high-frequency limit, ω is the angular frequency, and τ corresponds to the relaxation time. Within the RC microcircuit network, the conductive carbon fiber skeleton acts as the resistive pathway, while the carbon fiber surface and reduced graphene oxide layers serve as capacitor electrodes separated by dielectric insulating layers. Under an alternating electromagnetic field, interfacial charge accumulation occurs at these heterogeneous interfaces, forming numerous micro capacitive units. The time-lagged polarization response associated with capacitor charging and

discharging induces strong interfacial polarization and dielectric relaxation. Consequently, the coupled effects of conductive loss and polarization relaxation endow CF-300 with the highest dielectric loss factor (ε"). In addition, when the electrode interfaces of the micro capacitors are optimally matched, the RC network produces multiple relaxation superpositions, which significantly enhances the imaginary component of the complex permittivity. However, further increases in reduction temperature led to partial graphitization, which reduces defect density and weakens polarization processes, thereby diminishing the overall dielectric response.

As shown in Fig. 4b, the real part of the complex permeability (μ′) for all samples remains close to 1, while the imaginary component (μ″) is nearly 0, indicating negligible magnetic loss and confirming the dielectric-dominated nature of the composites. Consequently, microwave attenuation primarily originates from dielectric loss mechanisms. The dielectric loss tangent ($\tan\delta_\varepsilon = \varepsilon''/\varepsilon'$) further evaluates the electromagnetic energy dissipation capability. CF-300 exhibits the highest $\tan\delta_\varepsilon$ values across a broad frequency range (Fig. 4c), consistent with its significantly enhanced ε″ value and superior dielectric loss performance. This enhancement arises from the optimal balance between electrical conductivity and interfacial polarization within the hierarchical CF-HP-RGO structure. At moderate reduction temperatures, partially restored sp^2 conductive domains in RGO facilitate efficient charge transport along the conductive network, while abundant structural defects and heterogeneous interfaces provide numerous polarization centers. Meanwhile, the RGO interlayer achieves optimal interfacial matching with the carbon fiber surface, enabling the strongest dielectric relaxation response and enhanced electromagnetic energy dissipation.

The dielectric loss capability plays a crucial role in determining the ability of microwave-absorbing materials to attenuate incident electromagnetic waves. In particular, the attenuation constant (α), which quantitatively describes the decay of electromagnetic waves during propagation within the material, is widely used to

evaluate the intrinsic attenuation ability of absorbers [26]. The attenuation constant can be calculated according to Equation (6):

$$\alpha = \frac{\sqrt{2}\pi f}{c}\sqrt{(\mu''\varepsilon'' - \mu'\varepsilon') + \sqrt{(\mu''\varepsilon'' - \mu'\varepsilon')^2 + (\mu'\varepsilon'' + \mu''\varepsilon')^2}} \quad (6)$$

Here, f represents the electromagnetic wave frequency, c denotes the speed of light in vacuum, and μ' and μ'' correspond to the real and imaginary parts of the complex permeability, respectively. As conduction loss, interfacial polarization, and dielectric relaxation within the RC microcircuit network become more pronounced, the attenuation constant correspondingly increases, indicating stronger dissipation of electromagnetic energy during wave propagation within the absorber. A comparative analysis of the attenuation constants for five samples was conducted to further evaluate their electromagnetic energy dissipation capability (Fig. 4d). The attenuation constants of all samples increase gradually with frequency, indicating enhanced electromagnetic wave attenuation in the high-frequency region. Among them, CF-300 exhibits the highest attenuation constant over the entire frequency range, suggesting its superior microwave absorption capability.

The structural heterogeneity of the composite material leads to a broad distribution of relaxation times, which can be described by the Cole-Cole equation [27]:

$$\varepsilon^* = \varepsilon_\infty + \frac{\varepsilon_s - \varepsilon_\infty}{1 + (i\omega\tau)^{1-\alpha}} \quad (7)$$

To further clarify the relaxation mechanisms associated with the CF-HP-RGO interfacial microstructures with different reduction levels, Cole-Cole plots were analyzed for CF-200, CF-300, and CF-400 (Fig. 4e-g). According to Debye relaxation theory, each semicircular arc in the Cole-Cole plot corresponds to an individual dielectric relaxation process. Compared with CF-0 without thermal reduction, the thermally reduced CF@HP@RGO samples exhibit significantly enhanced dielectric relaxation behavior (Fig.S9). Upon thermal reduction, the removal of oxygen-containing functional groups and the formation of sp^2 microdomains lead to

increased conductivity and the generation of additional heterogeneous interfaces. These structural evolutions give rise to multiple relaxation processes, which are manifested as multiple semicircles in the Cole-Cole plots. This also contributes to improved impedance matching by balancing conduction and polarization effects, thereby enhancing electromagnetic wave absorption performance (Fig. S10). The Cole-Cole curve of CF-200 displays only one complete semicircle, which corresponds to interfacial polarization at the CF-HP interface. This result indicates that the low reduction degree of RGO does not generate significant polarization effects at the HP-RGO interface. In contrast, the Cole-Cole curve of CF-300 clearly exhibits two prominent semicircles and one smaller semicircle, corresponding to interfacial polarization at the CF-HP interface, polarization at the HP-RGO interface, and relaxation processes associated with the sp^2 microdomains within RGO, respectively. At a reduction temperature of 300 °C, the RGO layer and carbon fiber surface act as matched electrodes of the interfacial micro capacitor, producing the most pronounced relaxation response. For CF-400, the Cole-Cole plot shows two distinct semicircles, corresponding to polarization processes at the CF-HP interface and the HP-RGO interface. However, due to the higher reduction degree, sp^2 microdomains gradually coalesce and form more continuous graphitic domains, thereby reducing defect-induced polarization sites and weakening the relaxation behavior associated with sp^2 microdomains. To further investigate the effects of RGO flakes with different reduction degrees on the interfacial micro capacitor structure and the impedance matching performance of carbon fibers [28], the matching characteristics were evaluated using Equation (8-12):

$$\Delta = |sinh^2(Kfd) - M| \tag{8}$$

$$K = \frac{4\pi\sqrt{\varepsilon'\mu'}}{c cos\delta_\varepsilon cos\delta_\mu} sin\frac{\delta_\varepsilon + \delta_\mu}{2} \tag{9}$$

$$M = \frac{4\varepsilon' cos\delta_\mu \mu' cos\delta_\varepsilon}{(\mu' cos\delta_\varepsilon - \varepsilon' cos\delta_\mu)^2 + \left(tan\frac{\delta_\mu - \delta_\varepsilon}{2}\right)^2 (\mu' cos\delta_\varepsilon + \varepsilon' cos\delta_\mu)^2} \tag{10}$$

$$\delta_{\varepsilon} = arctan\frac{\varepsilon''}{\varepsilon'} \quad (11)$$

$$\delta_{\mu} = arctan\frac{\mu''}{\mu'} \quad (12)$$

where *f* represents the electromagnetic wave frequency, *c* denotes the speed of light in vacuum, and *d* corresponds to the absorber thickness. The calculated Δ reflects the compatibility between the intrinsic impedance of the absorber and that of free space; values approaching zero indicate better impedance matching and more efficient microwave penetration into the material. To further evaluate the impedance matching behavior of samples with different reduction degrees, two-dimensional distribution maps of the Δ were constructed for CF-200, CF-300, and CF-400 (Fig. 4h-j). In these maps, the deep red regions represent areas with optimal impedance matching. For CF-200, the deep red regions mainly appear at relatively large thicknesses and high frequencies, indicating that effective matching can only be achieved under limited conditions. In contrast, CF-300 exhibits deep red regions at thinner matching thicknesses, with well-distributed optimal matching zones across the 4-18 GHz frequency range, suggesting significantly improved impedance matching performance. For CF-400, the deep red regions again shift toward larger thicknesses and higher frequency regions, indicating relatively less favorable impedance matching. This optimized matching behavior in CF-300 originates from the improved interfacial compatibility between RGO and the carbon fiber surface, which enables the RC micro capacitor network to produce the strongest dielectric relaxation response. As a result, CF-300 simultaneously achieves enhanced dielectric loss, higher attenuation capability, more abundant relaxation processes, and more favorable impedance matching. Consequently, CF-300 demonstrates the most promising electromagnetic wave absorption performance among the investigated samples.

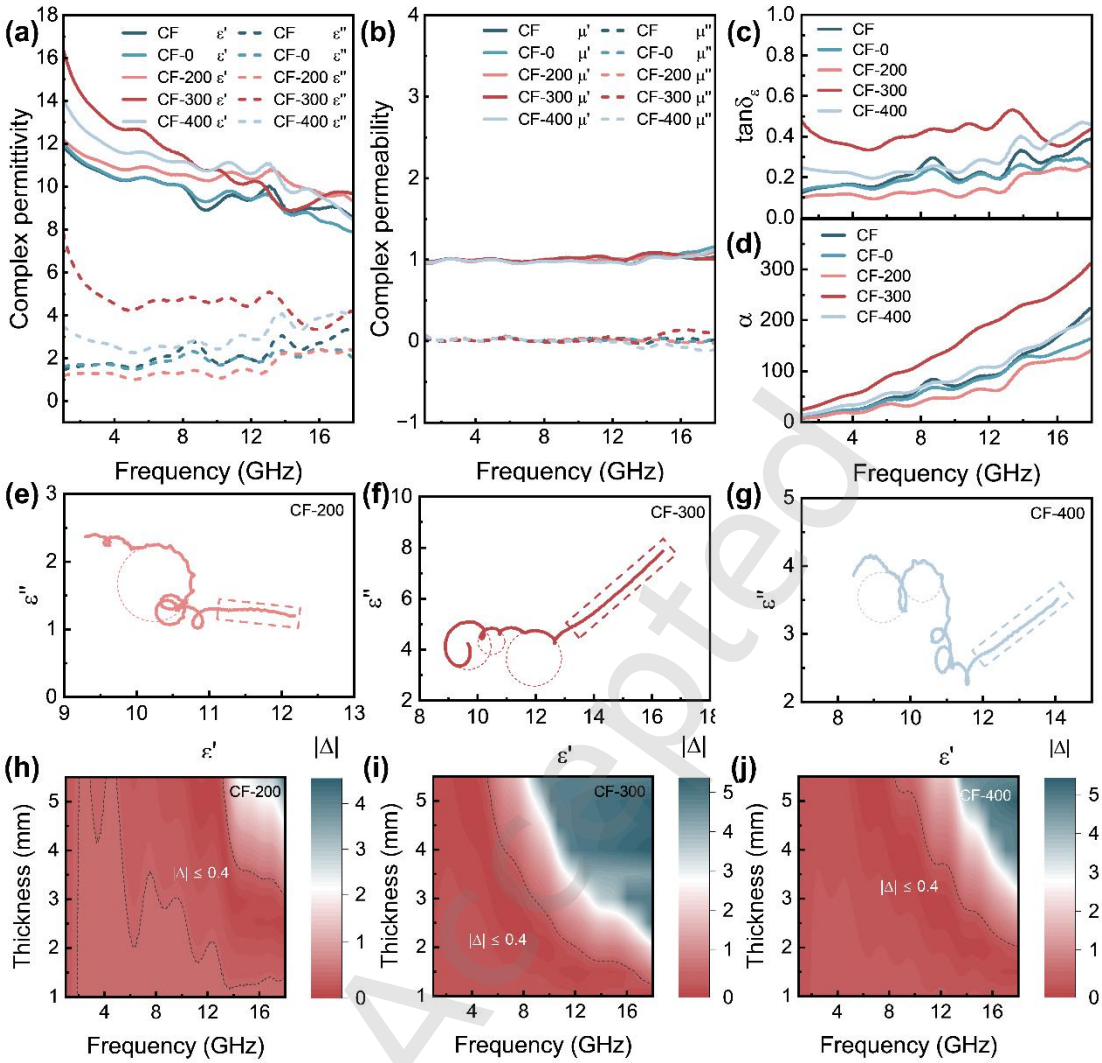

Figure 4. Electromagnetic parameter analysis of CF samples. (a) Complex permittivity (ε′, ε″). (b) Complex permeability (μ′, μ″). (c) Dielectric loss tangent ($\tan\delta_\varepsilon$). (d) Attenuation constant. Cole-Cole plots of (e) CF-200, (f) CF-300, and (g) CF-400. Two-dimensional Δ maps of (h) CF-200, (i) CF-300, and (j) CF-400.

The microwave absorption performance of the composites was evaluated based on transmission line theory. By correlating reflection loss (RL) with frequency and absorber thickness, the electromagnetic attenuation capability of the materials can be systematically assessed. Generally, RL ≤ −10 dB, corresponding to over 90% attenuation of incident electromagnetic waves, is considered the criterion for effective microwave absorption. The three-dimensional RL distributions as a function of

frequency and matching thickness provide an intuitive evaluation of the overall absorption capability. As shown in **Fig. 5**a, CF-200 exhibits relatively high RL, and strong absorption peaks mainly appear at larger matching thicknesses, indicating limited overall absorption performance. In contrast, the 3D RL distribution of CF-300 (Fig. 5d) presents stronger absorption peaks and a broader effective absorption region at relatively low thicknesses, demonstrating significantly improved microwave attenuation capability. For CF-400 (Fig. 5h), although a relatively wide effective absorption region can also be observed, the overall absorption intensity is weaker than that of CF-300. To further distinguish the absorption characteristics of different carbon fiber samples, two-dimensional RL contour maps were analyzed. The effective absorption bandwidth (EAB), defined as the frequency range where RL ≤ −10 dB, is a key parameter for evaluating microwave absorbers. As shown in Fig. S11a-d, strong absorption regions for all samples mainly appear in the high-frequency range. Notably, CF-300 exhibits the most outstanding absorption performance among all samples. At a matching thickness of 4.6 mm, CF-300 achieves a minimum RL of -42.5 dB. At a matching thickness of 1.6 mm, a maximum EAB of 5.24 GHz, covering almost the entire Ku-band, indicating excellent microwave attenuation capability. This remarkable enhancement demonstrates the effectiveness of the interfacial micro capacitor structure in improving the absorption performance of carbon fibers. To further investigate thickness-dependent absorption behavior, RL curves at matching thicknesses ranging from 1.6 to 3.2 mm were analyzed (Fig. 5b, e, i and Fig. S11e-f). With increasing absorber thickness, the frequency corresponding to the minimum RL gradually shifts toward lower frequencies, while the absorption intensity decreases slightly, which is consistent with the quarter-wavelength attenuation mechanism. Compared with other samples, CF-300 enables efficient microwave absorption across a wide frequency range (6.09-18 GHz) by simply adjusting the absorber thickness. In contrast, CF-200 only achieves effective absorption at high frequencies under relatively thin conditions, while CF-400 shows noticeably weakened RL peaks

compared with CF-300. Further analysis of the maximum EAB values for all samples reveals a distinct trend during the reduction process. At the initial reduction stage, the EAB becomes narrower, which may be attributed to the absence of sp^2 microdomains and the reduction of oxygen-containing functional groups, leading to insufficient polarization centers. When the reduction temperature reaches 300 °C, the formation of sp^2 microdomains significantly enhances dielectric relaxation and interfacial polarization, thereby markedly expanding the effective absorption bandwidth. However, after further reduction at 400 °C, the gradual coalescence of sp^2 domains reduces defect-induced polarization sites, resulting in a decrease in EAB (Fig. 5c). Similarly, comparison of the minimum RL values indicates that the microwave absorption capability of the composites first increases and then decreases during the reduction process, with CF-300 exhibiting the strongest absorption performance. These results demonstrate that the optimized CF-HP-RGO interfacial micro capacitor structure at 300 °C effectively regulates dielectric loss, relaxation processes, and impedance matching, thereby enabling superior microwave absorption performance.

To further evaluate the absorption efficiency of carbon fibers under practical conditions of limited thickness and filler loading, the specific reflection loss (SRL) and specific effective absorption bandwidth (SEAB) were calculated. SRL characterizes the normalized absorption intensity considering both absorber thickness and filler ratio, whereas SEAB represents the effective bandwidth efficiency per unit thickness. The corresponding values were determined using Equations (13) and (14):

$$SRL = \frac{|RL_{min}|}{t \times loading} \times 10^{-2} \quad (13)$$

$$SEAB = \frac{EAB}{t \times loading} \times 10^{-2} \quad (14)$$

Here, *t* represents the absorber thickness, while *loading* denotes the mass fraction of

the filler. The optimized CF@HP@RGO composite exhibits high SRL and SEAB values, demonstrating that efficient microwave attenuation can be maintained even at relatively small absorber thicknesses. In addition, compared with many previously reported carbon-based microwave absorbers, this material displays superior broadband absorption efficiency (Table S1). Therefore, CF@HP@RGO is characterized by strong reflection loss and wide effective bandwidth under thin-layer conditions, highlighting its promising potential for practical electromagnetic wave absorption applications [29-42].

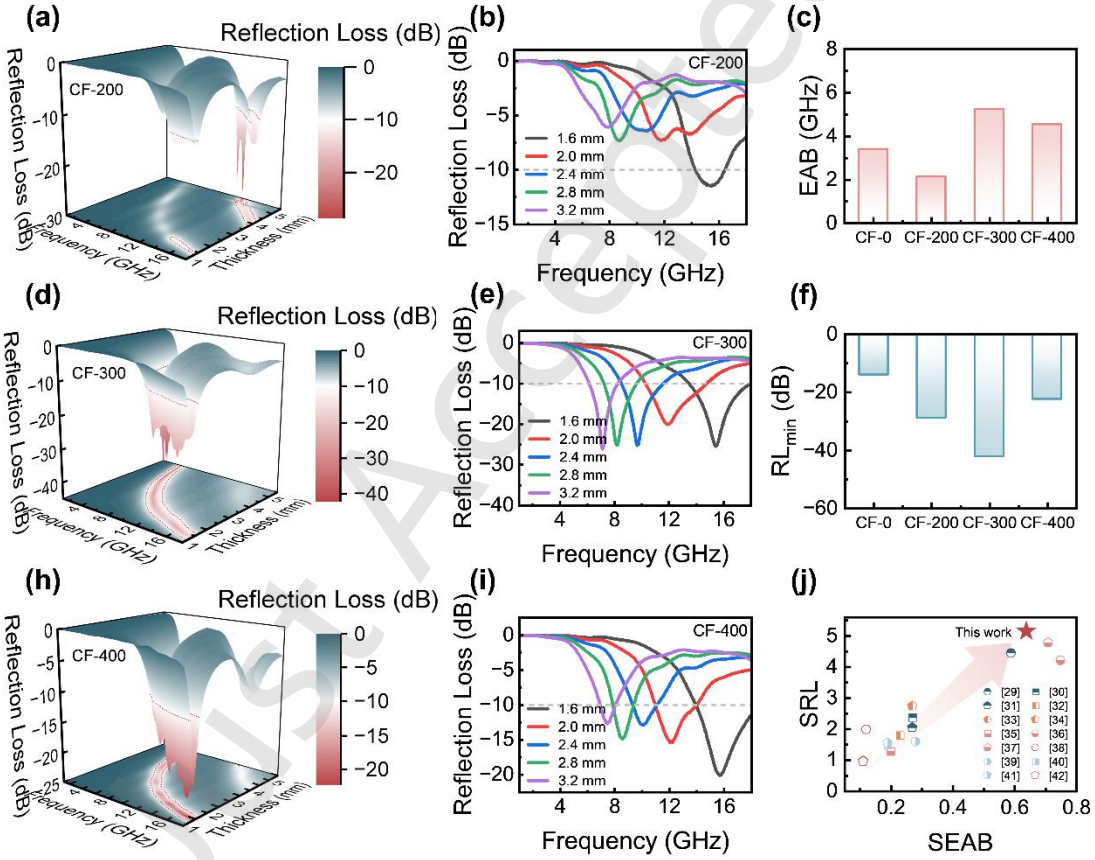

Figure 5. Microwave absorption performance of carbon fiber composites. (a) Three-dimensional RL distribution and (b) RL curves as a function of thickness for CF-200.

(c) Comparison of the maximum effective absorption bandwidth (EAB) of the four samples. (d) Three-dimensional RL distribution and (e) RL curves at selected thicknesses for CF-300. (f) Minimum RL values of the four samples. (g)

Three-dimensional RL distribution and (h) RL curves at selected thicknesses for CF-400. (i) Performance comparison with recently reported microwave absorbers.

3.3 RC Microcircuit-Induced Dielectric Loss and Microwave Attenuation Mechanism

Carbon fibers, HP, and reduced graphene oxide (RGO) collectively form a heterogeneous conductive-dielectric-conductive interface architecture. From a cross-sectional perspective, the interior of the carbon fiber acts as a resistive element, while the carbon fiber surface and the RGO coating, separated by the HP dielectric layer, function as the two electrodes of a micro capacitor. Consequently, the resulting core-shell configuration can be conceptualized as an array of interconnected RC microcircuits [43, 44]. This RC microcircuit network plays a crucial role in regulating dielectric loss and electromagnetic wave attenuation. As discussed above, the reduction degree of the RGO coating increases with increasing thermal reduction temperature. With progressive reduction, sp^2 microdomains gradually form and expand, accompanied by a decrease in the O/C atomic ratio and the gradual removal of oxygen-containing functional groups (**Fig. 6**a). Meanwhile, the ~80 nm thick HP dielectric layer provides an effective medium for electromagnetic wave scattering within the coating, thereby prolonging the propagation path of incident waves and enhancing energy dissipation. For a typical micro capacitor unit [45, 46], its capacitance can be described by the classical parallel-plate capacitor equation (Equation 15) (Fig. 6b):

$$C = \varepsilon \frac{A}{d} \quad (15)$$

Here, C denotes the capacitance of the micro capacitor, A represents the effective electrode area, and d is the thickness of the dielectric layer. The parameter $\varepsilon = \varepsilon_r \varepsilon_0$ corresponds to the permittivity of the dielectric medium, where ε_r and ε_0 represent the relative permittivity and vacuum permittivity, respectively. Based on this configuration, the resistance across the dielectric layer can be expressed as Equation

(16):

$$R = \rho\frac{d}{A} \quad (16)$$

Here, R denotes the resistance, while ρ represents the electrical conductivity of the dielectric layer. Based on the relationship between resistance and capacitance, the relaxation time of the RC circuit can be expressed by Equation (17):

$$\tau = RC \quad (17)$$

By substituting Equations (15) and (16) into Equation (17):

$$\tau = \rho\varepsilon \quad (18)$$

This result indicates that the relaxation time is primarily governed by the intrinsic electrical properties of the material and is essentially independent of the geometric dimensions of the capacitor. For typical carbon-based composites, the electrical resistivity generally ranges from 10^{-3} to 10^{-1} Ω·m, while the relative permittivity of macromolecular polymer dielectrics is typically in the range of 5 to 15 [47]. Based on these parameters, the relaxation time (τ) is estimated to be on the order of 10^{-11}~10^{-10} s. Accordingly, the corresponding resonance response frequency can be calculated using Equation (17):

$$f = \frac{1}{2\pi\tau} \quad (19)$$

By estimating the response frequency from the theoretical relaxation time range, it can be found that the calculated frequency falls well within the microwave region, particularly the X and Ku bands (8-18 GHz). This indicates that the RC microcircuit arrays formed within the composite can effectively trigger dielectric relaxation under

microwave irradiation, thereby enabling efficient attenuation of electromagnetic waves within these frequency ranges. According to the Debye relaxation model, the strongest polarization hysteresis occurs when the relaxation time is comparable to the period of the incident electromagnetic wave. Under this condition, the RC microcircuit arrays can effectively promote dielectric relaxation processes, leading to an enhanced imaginary part of the complex permittivity (ε″) and consequently improved microwave energy dissipation capability. Therefore, the presence of the RC microcircuit array structure plays a critical role in enhancing dielectric loss and microwave absorption performance in the CF@HP@RGO system (Fig. 6c).

At the same time, Maxwell-Wagner interfacial polarization forms at the CF-HP-RGO interface (Fig. 6d). In heterogeneous composite materials containing conductive and dielectric phases, the adjacent components exhibit differences in electrical conductivity and permittivity [48]. This leads to significant charge accumulation at the interface. The polarization intensity can be expressed by Equation (20):

$$P = \varepsilon_0 \chi E \quad (20)$$

Here, P represents the polarization intensity, χ denotes the electric susceptibility, and E is the electric field intensity. In the present composite system, numerous heterogeneous interfaces are formed among the carbon fibers (CF), RGO nanosheets, and the HP dielectric layer, which serve as effective polarization centers. Under incident electromagnetic irradiation, electrons migrate along the conductive network and accumulate at these heterogeneous interfaces, resulting in pronounced interfacial polarization and dielectric relaxation processes. Moreover, the nanoscale dielectric layer within the micro capacitor structure can generate significant local electric field enhancement. Such localized electric field amplification further promotes charge accumulation and polarization intensity at the interfaces, thereby strengthening dielectric loss [49]. The electric field intensity within the micro capacitor can be

expressed using Equation (21):

$$E = \frac{V}{d} \quad (21)$$

Here, V represents the potential difference across the dielectric layer, and d denotes the thickness of the dielectric layer. When the dielectric layer thickness reaches the nanoscale, the local electric field strength can be significantly amplified. In the present system, the HP dielectric layer has a thickness of only ~80 nm, which theoretically leads to a local electric field enhancement of approximately three to four orders of magnitude within the micro capacitor structure. Such intense electric field concentration greatly promotes charge accumulation and polarization at the heterogeneous interfaces, thereby enhancing dielectric relaxation and increasing the imaginary part of the complex permittivity (ε″). As a result, the dielectric loss capability is significantly improved, facilitating efficient attenuation of incident electromagnetic waves.

In addition to polarization relaxation, conduction loss also plays an important role in electromagnetic wave attenuation. In the present composite system, a continuous conductive network is formed both within the carbon fibers and along the RGO coating, which facilitates efficient electron transport under an alternating electromagnetic field. During this process, the migration and hopping of charge carriers within the conductive pathways lead to energy dissipation in the form of conductive loss. The relationship between electrical conductivity and dielectric loss can be described by Equation (22)[50]:

$$\varepsilon'' = \frac{\sigma}{\varepsilon_0 \omega} \quad (22)$$

Here, σ represents the electrical conductivity of the material. A higher electrical conductivity indicates that more charge carriers participate in transport processes

during electromagnetic wave propagation, resulting in enhanced carrier migration and collision, which ultimately converts electromagnetic energy into thermal energy through Joule heating (Fig. 6e). This process contributes significantly to conduction loss and promotes the attenuation of incident electromagnetic waves [51, 52].

Based on the above analysis, the mechanisms responsible for the enhanced microwave absorption performance of CF@HP@RGO can be summarized as follows:

(1) Conductive loss: Interconnected conductive pathways are established within the carbon fibers and the RGO nanosheets, forming an efficient conductive network. Under an alternating electromagnetic field, electrons migrate and oscillate along these conductive channels, dissipating electromagnetic energy through resistive loss and Joule heating.

(2) RC microcircuit arrays: The CF-HP-RGO heterogeneous structure forms numerous RC microcircuit arrays. When electromagnetic waves are incident, periodic charge accumulation and release occur within these microcircuits, inducing dielectric relaxation processes that significantly enhance electromagnetic wave attenuation.

(3) Polarization loss: Carbon fibers and RGO-300 act as conductive phases, while the HP layer functions as a dielectric medium, forming heterogeneous conductive–dielectric interfaces. The large contrast in dielectric properties induces strong interfacial charge accumulation, resulting in Maxwell-Wagner interfacial polarization. Meanwhile, the complex interface structure also promotes multiple scattering of electromagnetic waves, thereby prolonging the propagation path and further enhancing energy dissipation.

In summary, the CF@HP@RGO composite forms a dense array of RC microcircuits through its heterogeneous conductive–dielectric–conductive interface structure. This architecture synergistically enhances conductive dissipation, interfacial polarization, dielectric relaxation, and local electric field amplification, resulting in substantially increased complex permittivity and dielectric loss capability. Consequently, the

composite exhibits efficient electromagnetic wave attenuation and broadband absorption within the X and Ku band region. These results demonstrate that constructing an RC microcircuit array via an interfacial micro capacitor architecture is an effective strategy for achieving efficient broadband microwave absorption.

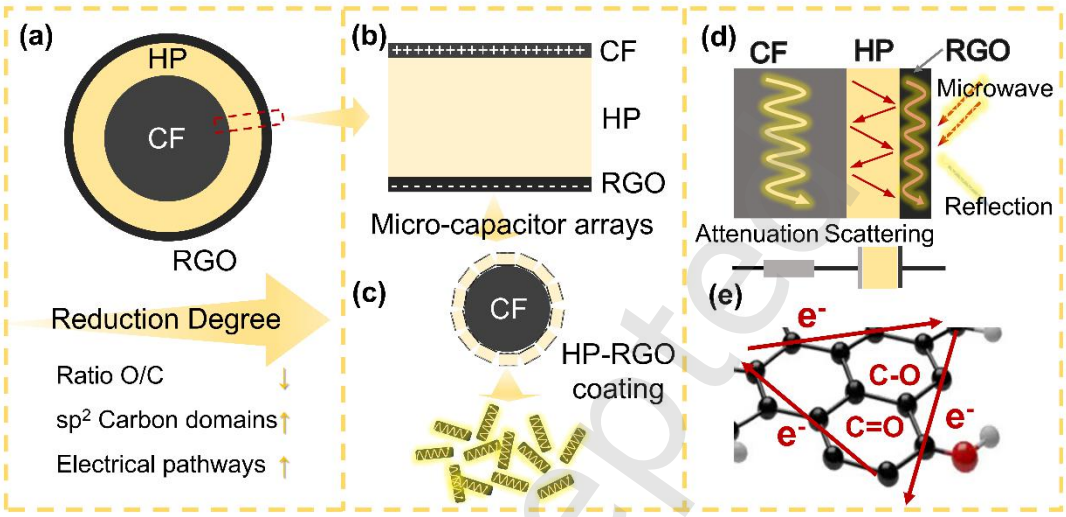

Figure 6. Schematic illustration of the electromagnetic wave absorption mechanism of CF@HP@RGO. (a) Electromagnetic wave scattering. (b) Interfacial micro capacitor structure. (c) RC circuit array. (d) Equivalent RC circuit model. (e) sp^2 microdomain–accelerated electron transport.

4. Conclusions

This work presents the design of a CF@HP@RGO composite microwave absorber based on the construction of an RC microcircuit array for efficient electromagnetic wave attenuation. In this architecture, conductive carbon fibers and the RGO sheet network provide continuous electron transport pathways, while the carbon fiber surface, together with the HP dielectric layer and RGO nanosheets, forms a micro capacitor structure. This configuration, combined with the conductive carbon fiber core, constitutes an RC equivalent microcircuit network. Benefiting from this microcircuit array architecture, the optimized composite exhibits outstanding microwave attenuation capability. At a matching thickness of 1.6 mm and a filler loading of only 5 wt.%, CF-300 achieves an effective absorption bandwidth (EAB) of

up to 5.24 GHz. Compared with most previously reported carbon-based absorbers, particularly carbon fiber absorbers, the CF-300 developed in this work achieves near-complete coverage of the Ku band under thinner thickness and lower filler loading conditions. This superior absorption performance originates from the synergistic effects of conductive loss within carbon fibers, relaxation polarization induced by the RC microcircuit arrays, and interfacial polarization at heterogeneous interfaces. These mechanisms collectively enhance dielectric loss and electromagnetic wave attenuation within the composite material. This work demonstrates that engineering interfacial micro capacitor structures offers an effective strategy for developing lightweight carbon-fiber-based microwave absorbers with thin thickness and broadband attenuation capability.

Acknowledgments

This work was supported by National Natural Science Foundation of China (NSFC 52372041, 52432002, 525B2034, 52402369) and Sichuan Science and Technology Program (No. 2025ZDZX0017). Special thanks to HIT Center for Analysis and Measurement and Dr. Zheng Zhen for the electron microscope test analysis.

Conflict of Interest

The authors declare no conflict of interest.

Author Contribution Statement

B. S. G.: Writing – original draft, visualization, data curation, experimental design. Y. F. Y. and J. Z. H.: Data curation, visualization, software. T. C. and N. Y. J.: Data curation, software. X. H.: Investigation, software. X. X. H.: Writing – review &editing, validation. H. T. Y. and D. C. J.: Validation. Y. Z.: Writing – review & editing, funding acquisition, validation, methodology. All the authors have approved the final manuscript.

Reference

[1] Wang, J; Song, T. L; Ming, W; Yele, M. X; Chen, L. F; Zhang, H; Zhang, X. J; Liang, B. L; Wang, G. S. High MXene loading, nacre-inspired MXene/ANF electromagnetic interference shielding composite films with ultralong strain-to-failure and excellent Joule heating performance. Nano Res. 2024, 17, 2061-9.

[2] Wang, J. Hao; Cai, B; Sun, B. W; Hou, Z. L; Yang, S. H; Yang, Q. L; Zhao, P. Y; Li, W. P; Zhang, Y;. Wang, G. S. Molecular dipole engineering for tailored dielectric properties in MXene/ZnO heterostructures. Acta Physico-Chimica Sinica, 2026, 100271.

[3] Liu, P. B; He, Z. Z; Li, X. C; Ding, L. F; Liu, S, H; Kong J. Multifunctional Hollow Carbon Microspheres Enable Superior Electromagnetic Wave Response and Corrosion Barrier. Adv. Mater., 2025, 37, 2500646.

[4] Wu, Q. Q; Ma, Z. L; Wang, C. Y; Tao, Y; Wang S. Y; Jin, Z. Y; Gao, T. D; Li, C; Liu P. B. Carbon nanofibers with small-sized Co nanoparticles and structural defects via a confined-coordination growth strategy toward electromagnetic wave absorption. J. Adv. Ceram., 2025, 14, 9221210.

[5] Qi, J. M; Liang, C. B; Ruan, K. P; Li, M. K; Guo, H; He, M. K; Qiu, H; Guo, Y. Q; Gu, J. W. Cactus-like Architecture for Synergistic Microwave Absorption and Thermal Management. Natl. Sci. Re. 2025, 12: nwaf394.

[6] Wang, J; Ming, W; Chen, L.F; Song, T. L; Yele, M. X; Zhang, H; Yang, L; Sarula, G; Liang, B. L; Yan, L. T; Wang, G. S. MoS_2 Lubricate-Toughened MXene/ANF Composites for Multifunctional Electromagnetic Interference Shielding. Nano-Micro Lett, 2025, 17: 36.

[7] He, Z. Z; Xu, H. X; Shi, L. Z; Ren, X. R; Kong, J; Liu, P. B. Hierarchical Co_2P/CoS_2@C@MoS_2 Composites with Hollow Cavity and Multiple Phases Toward Wideband Electromagnetic Wave Absorption. Small 2024, 20, 2306253 .

[8] Zhong, X; Gu, J. W. Core-shell Co-C@CNT engineered to enable concurrent

thermal conductivity and microwave absorption for Poly(4, 4′-dihydroxybiphenyl isophthalate). Trans. Mater. Res. 2026, 2, 100184.

[9] Zhan, B. B; Zhang, Y. R; Tan, Z. Y; Xie, A. M; Gong, X; Peng, Q; Yang, J. L; Qu, Y. P; Qi, X. S. Multi-dimensional, multi-interfacial, and multi-path synergy enables broadband absorption, corrosion resistance, Joule heating, and thermal performances in hierarchical carbon/Ni nanoparticles-carbon nanocoils foams. InfoMat 2026, 8, e70098

[10] Yele, M. X; Sarula, G; Yang, J; Yang, L; Zhang, H; Chen, L. F; Zhang, X. M; Wang, J. H; Wang, T. Y; Jin, C. Z; Liang, B. L; Yan, L. T. Integrated structural-functional MXene-GNs/ANF flexible composite film with enhanced thermal conductivity and electromagnetic interference shielding performance. J. Mater. Sci. Technol. 2026, 241, 200-210.

[11] Xu, F. F; Cai, B; Sun, X. B; Zhang, Y; Bai, S; Liang, C. M; C. Koo, M; Bai, Y. X; Zhao, P. Y; W, G. S. A strategy for modulation of permittivity in manganese doping to induce lattice distortion. InfoMat, 2026, 8(6), e70087..

[12] Xiao, J. X; Zhan, B. B; Tan, Z. Y; Ding, J. F; Qu, Y. P; Gong, X; Peng, Q; Zhong, W; Chen, Y. L; Qi, X. S. Integration of photo-driven rapid self-healing and environmental robustness for durable electromagnetic wave absorbing elastomers. InfoMat.2026, e70127.

[13] He, M. K; Hu, J. W; Yan, H; Zhong, X; Zhang, Y. L; Liu, P. B; Kong, J; Gu, J. W. Shape Anisotropic Chain-like CoNi/Polydimethylsiloxane Composite Films with Excellent Low-frequency Microwave Absorption and High Thermal Conductivity. Adv. Funct. Mater. 2025, 35, 2316691.

[14] Lu, Z; Wang, Y; Di, X. C; Wang, N; Cheng, R. R; Yang, L. Q. Heterostructure design of carbon fiber@graphene@layered double hydroxides synergistic microstructure for lightweight and flexible microwave absorption. Carbon. 2022, 197, 466-475.

[15] Yang, L. Y; Wang, L. M; Dong, S; Chen, G. Q; Hong, C. Q; Zhang, X. H; Zhou,

Y. C. Lightweight C_f/HC-SiBCN composite for multifunctional applications. J Adv Ceram. 2025, 14, 9221068.

[16] Wang, H. M; Zhan, B. B; Zhang, Y. R; Tan, Z. Y; Ding, J. F; Chen, Y. L; Qu, Y. P; Qi, X. S. Multi-scale synergistic regulation strategy to develop mesoporous carbon hollow nanospheres/bean-shaped nanofibers for corrosion resistance, flexible and lightweight microwave absorbers. Research, 2025, 9(1): 1051.

[17] Guo, Y. Q; Li, P; Zhao, R. L; Gu, J. W. Preparation and mechanism of thermally conductive polyimide phase change composites with electromagnetic wave-absorbing performance. Acta Polymerica Sinica, 2025, 56(12), 2347-2360.

[18] Guo, Z. Q; Zhang, X. Y; Lv, C. P; Zhang, S. Y; Gao, Z. G; Jia, Z. R; Lan, D; Wu, G. L. Advantageous synergistic strategy to construct Ni@C/PC composites for efficient electromagnetic wave absorption. Carbon. 2025, 234, 120010.

[19] Zhao, R; Liang, B. Q; Shi, Y. X; Dong, Q; Li, T. X; Gu, J. W; Ma, Y; Zhang, J; Melhi, S; Alshammari, A. S; El-bahy, Z. M; Guo, Z. H. Recent progress of carbon-based magnetic fibers for electromagnetic wave absorption. Carbon. 2024, 229, 119513.

[20] Zong, J. Y; Zhai, H. Z; Guan, H. Z; Wang, Z. Z; Cao, M. S; Cao, W. Q. Host-Guest Engineered Electromagnetic Fabrics with Controllable Polarization-Conduction Network for Multispectral Stealth and Wireless Actuation. Adv. Funct. Mater. 2025, 35, e07277.

[21] Wu, Q. Q; Ma, Z. L; Wang, C. Y; Tao, Y; Wang, S. Y; Jin, Z. Y; Gao, T. D; Li, C; Liu, P. B. Carbon nanofibers with small-sized Co nanoparticles and structural defects via a confined-coordination growth strategy toward electromagnetic wave absorption. J Adv Ceram. 2025, 14, 9221210.

[22] He, Y. F; Liu, D. D; Dou, S. H; Ma, L; Dan, Z. Y; Yang, M. H; Zhong, B; Xia, L; Huang, X. X. Interface-engineered decoupled conductivity and relaxation: Synergistic modulation of Debye-parameters in N-doped SiO_2/MXene broadband wave-absorbing materials. J Adv Ceram. 2025, 14, 9221150.

[23] Ding, L. F; He, Z. Z; Zhang, R. N; Liu, S. H; Geng, W. C; Liu, P. B. Hollow $Zn_{1-x}Co_{2-y}Ni_xFe_yO_4$ spinel via multi-metal ion doping: ultralight and broadband microwave absorber. Soft Science, 2026, 6, 2.

[24] Hong, J. M; Kang, Y. S; Jang, J; Kim, U. Y. Analysis of facilitated transport in polymeric membrane with fixed site carrier 2. Series RC circuit model. J. Membr. Sci. 1996, 109, 159-163.

[25] Su, X. G; Wang, J; Liu, T; Zhang, Y; Liu, Y. N; Zhang, B; Liu, Y. Q; Wu, H. J; Xu, H. X. Controllable Atomic Migration in Microstructures and Defects for Electromagnetic Wave Absorption Enhancement. Adv. Funct. Mater. 2024, 34, 2403397.

[26] Xiang, Z. N; Wang, Y. Q; Yin, X. M; He, Q. C. Microwave absorption performance of porous heterogeneous SiC/SiO_2 microspheres. Chem. Eng. J. 2026, 451, 138742.

[27] Yan, Y. F; Qin, G. Y; Zhang, K. L; Gao, B. S; Ma, G. S; Huang, X. X; Zhou, Y. Enhancing microwave absorption performance of MoS_2 by synergistic effect of Fe doping. J Adv Ceram. 2025, 14, 9221039.

[28] He, M. K; Zhong, X; Lu, X. H; Hu, J. W; Ruan, K. P; Guo, H; Zhang, Y. L; Guo, Y. Q; Gu, J. W. Excellent Low-Frequency Microwave Absorption and High Thermal Conductivity in Polydimethylsiloxane Composites Endowed by Hydrangea-Like CoNi@BN Heterostructure Fillers. Advanced Materials, 2024, 36, 2410186.

[29] Zhao, Y. P; Zuo, X. Q; Guo, Y; Huang, H; Zhang, H; Wang, T; Wen, N. X; Chen, H; Cong, T. Z; Muhammad, J; Yang, X; Wang, X. N; Fan, Z; Pan, L. Structural Engineering of Hierarchical Aerogels Comprised of Multi-dimensional Gradient Carbon Nanoarchitectures for Highly Efficient Microwave Absorption. Nano-Micro Lett. 2021, 13:144.

[30] Zhou, L; Hu, P. F; Bai, M; Leng, N; Cai, B; Peng, H, L; Zhao, P. Y; Guo, Y. Q; He, M. K; Wang, G. S; Gu, J. W. Harnessing the Electronic Spin States of Single Atoms for Precise

Electromagnetic Modulation. Adv. Mater., 2025, 37, 2418321.

[31] Zhang, B; Qu, Z. Y; Ruiz-Agudo, C; Yang, L; Chi, B. H; Kong, Y; Wang, F. Z. Lightweight magnetic carbon nanotube/cellulose nanofibre aerogels with microstructure engineering for enhanced microwave absorption. Carbon. 2025, 234, 120020.

[32] Han, X. J; Feng, Y. F; Zhang, N; Du, W; Zhang, W. L; Yu, Q. Q; Liu, Y. F; Wang, B; Jiang, F. Y; Liu, L. Y; Xu, L. N; Zhang, X. Y. Bio-based multifunctional carbon aerogels for ultrawide electromagnetic wave absorption and thermal insulation. Carbon. 2025, 238, 120231.

[33] Feng, S. L; Yang, Y. G; Wang, J. M; Wang, Y; Zhou, X. T. Improved mechanical properties and fracture mechanism of C/C composites with salt treatment monitored by synchrotron-based in-situ tensile XRD. Compos. Part B: Eng. 2020, 199, 108274.

[34] Ahmad, HS; Hussain, T; Nawab, Y; Salamat, S. Effect of various dielectric and magnetic nanofillers on microwave absorption properties of carbon fiber reinforced composites structures. Ceram Int. 2022, 48, 19882.

[35] Chen, X. T; Wu, Y; Gu, W. H; Zhou, M; Tang, S. L; Cao, J. M; Zou, Z. Q; Ji, G. B. Research progress on nanostructure design and composition regulation of carbon spheres for the microwave absorption. Carbon. 2022, 189, 617-633.

[36] Gao, Y; Lei, Z. K; Pan, L. N; Wu, Q; Zhuang, X. H; Tan, G. G; Ning, M. Q; Man, Q. K. Lightweight chitosan-derived carbon/rGO aerogels loaded with hollow $Co_{1-x}Ni_xO$ nanocubes for superior electromagnetic wave absorption and heat insulation. Chem. Eng. J. 2023, 457, 141325.

[37] Guo, Y; Wang, D. L; Tian, Y; Wang, J. W; Bai, T. T; Liu, H; Guo, Z. H; Liu, C. T; Shen, C. Y. FeCo alloy nanoparticle decorated cellulose based carbon aerogel as a low-cost and efficient electromagnetic microwave absorber. J. Mater. Chem. C. 2022, 10, 126-134.

[38] Negi, P; Joshi, S. K; Baskey, H. B; Kumar, S; Mishra, A. K; Kumar, A. Excellent

microwave absorbing performance of biomass-derived activated carbon decorated with in situ-grown $CoFe_2O_4$ nanoparticles. Mater. Adv. 2022, 3, 2533-2545.

[39] Liu, S. J; Wang, J; Zhang, B; Su, X. G; Chen, X; Chen, Y. H; Yang, H; Wu, Q. L; Yang, S. Transformation of traditional carbon fibers from microwaves reflection to efficient absorption via carbon fiber microstructure modulation. Carbon. 2024, 219, 118802.

[40] Chen, Q. Y; Chen, Z. Y; Ali, A; Luo, Y. Q; Feng, H. Y; Luo, Y. Y; Tsiakaras, P; Shen, P. K. Shell-thickness-dependent Pd@PtNi core-shell nanosheets for efficient oxygen reduction reaction. Chem. Eng. J. 2022, 427, 131565.

[41] Lou, G. B; Pei, G; Wu, Y. T; Lu, Y. Z; Wu, Y. T; Zhu, X. Q; Pang, Y. J; Shen, Z. H; Wu, Q; Fu, S. Y; Chen, H. Combustion conversion of wood to N, O co-doped 2D carbon nanosheets for zinc-ion hybrid supercapacitors. Chem. Eng. J. 2021, 413, 127502.

[42] Du, W. L; Chen, G. Z; Wang, X. S; Gu, J. W. Enhancing electromagnetic parameter modeling of irregularly shaped composite structures with partitioned equivalent modeling and near-field scanning. Chinese Journal of Electronics. 2026, 35, 1-15.

[43] Cao, M. S; Song, W. L; Hou, Z. L; Wen, B; Yuan, J. The effects of temperature and frequency on the dielectric properties, electromagnetic interference shielding and microwave-absorption of short carbon fiber/silica composites. Carbon. 2010, 48, 788-796.

[44] Wang, C. X; Liu, Y; Jia, Z. R; Zhao, W. R; Wu, G. L. Multicomponent Nanoparticles Synergistic One-Dimensional Nanofibers as Heterostructure Absorbers for Tunable and Efficient Microwave Absorption. Nano-Micro Lett. 2022, 15:13.

[45] Du, Z. R; Zhang, G. Y; Chen, K; Zhou, C; Zhu, X. S; Zhang, Y. X; Chen, K; Mi, H. Y; Wang, Y. M; Liu, C. T; Shen, C. Y. MXene/Polylactic Acid Fabric-Based Resonant Cavity for Realizing Simultaneous High-Performance Electromagnetic

Interference (EMI) Shielding and Efficient Energy Harvesting. ACS Appl. Mater. Interfaces. 2022, 14, 14607-14617.

[46] Chen, J; Luo, Q; Huang, J; He, Q; Sun, P; Du, X. Analysis and Design of an RC Snubber Circuit to Suppress False Triggering Oscillation for GaN Devices in Half-Bridge Circuits. IEEE TRANSACTIONS ONPOWERELECTRONICS. 2020, 35, 2704.

[47] Cai, B; Hou, Z. L; Qi, Y. Y; Zhao, P. Y; Peng, H. L; Zhang, Y; C. Koo, M; Yue, T. C; Hu, P. F; Liu, L. M; Wang, G. S. Facet-modulated ferroelectric polymers. Nature Communications, 2026, 17, 2065.

[48] Zhou, L; Wang, H. Y; Guo, Y. Q; Bai, M; Leng, N; Sun, X. B; Wang, G. S; Gu, J. W. Near-perfect light-capture materials with high environmental stability. Science China Materials, 2026.

[49] Ma, G. S; Liu, Y. H; Zhang, K. L; Qin, G. Y; Yan, Y. F; Zhang, T; Huang, X. X. Shape-tunable vanadium selenide/reduced graphene oxide composites with excellent electromagnetic wave absorption performance, carbon, 2025, 232, 119795.

[50] Meng, Y. T; Cai, B; Zhou, Y. T; Zhou, L; Zhang, Y; Wang, J. H; Sarula, G; Yan, L. T; Lu, M; Liang, B. L; Wang, G. S. Bionic coral reef inspired enhanced scattering of trimetallic LDH self assembled $Ti_3C_2T_x$ MXene for advanced microwave absorption. Nano Res. 2025, 18, 94907842.

[51]Gao, B. S; Yan, Y. F; Zhang, K. L; Liu, D. D; Huang, X. X. UltralightBroadbandElectromagneticWaveAbsorption Enabled by Interface-EngineeredTwo-layeredPeriodic Carbon Fiber Fabrics. Adv. Funct. Mater., 2026, 0, e32108.

[52] Shi, Z. X; Dong, T. N; Hu, H. M; Quan, J. R; Guan, Y. T; Xu, B. Q; Hang, Z. S; Wu, C. Developments in the integrated modification of mechanical and electromagnetic characteristics of SiC-based ceramics. Adv Ceram. 2025, 46, 1005-1198. (in Chinese)

Electronic Supplementary Material

Interfacial micro-capacitor engineering in CF/hyperbranched polyamide/RGO composites for efficient microwave absorption

Boshi Gao[1,2,3], Yuefeng Yan[1,2,3*], Xin Huang[4], Jingzhe Hong[1,2,3], Tao Chen[1,2,3], Naiyu Jiang[5*], Haitang Yang[4*], Dechang Jia[1,2,3], Yu Zhou[1,2,3], and Xiaoxiao Huang[1,2,3*]

1. MIIT Key Laboratory of Advanced Structural-Functional Integration Materials & Green, Manufacturing Technology, Harbin Institute of Technology, Harbin 150001, China

2. School of Materials Science and Engineering, Harbin Institute of Technology, Harbin 150001, China

3. National Key Laboratory of Precision Welding & Joining of Materials and Structures, Harbin Institute of Technology, Harbin 150001, China

4. AVIC Chengdu Aircraft Industrial (Group) CO., LTD., Chengdu 610092, China

5. Institute of Composite Materials and Structures, Harbin Institute of Technology, Harbin 150001, China

*Address correspondence to Xiaoxiao Huang, swliza@hit.edu.cn; Yuefeng Yan, 22B909026@stu.hit.edu.cn; Haitang Yang, 371136039@qq.com; Naiyu Jiang, jiangnaiyu0904@163.com

Supporting information to https://doi.org/10.26599/NR.2026.94908703

Experimental Section:

Finite Element Analysis of Loss Field at the CF@HP@RGO Interface:

Finite element analysis (FEA) was employed to simulate the loss field distribution at the CF@HP@RGO interface. A two-dimensional axisymmetric model was constructed to represent the interfacial structure. In this model, the interior region was defined as carbon fiber, with the left boundary representing the carbon fiber interface and the right boundary corresponding to the RGO interface within the rectangular cross-section. Both interfaces were treated as open boundaries, while periodic boundary conditions were applied along the upper and lower boundaries of the model. The obtained two-dimensional axisymmetric solution was revolved around the Z-axis to reconstruct the three-dimensional loss field distribution. The intrinsic electrical parameters of the carbon fiber and HP dielectric layer were considered constant, whereas the electrical conductivity of the RGO coating was varied (50, 400, and 1000 $S \cdot m^{-1}$) based on reported theoretical and experimental values[1-4]. This model enables the quantitative evaluation of interfacial loss behavior as a function of RGO conductivity, providing insight into the role of the micro capacitor structure in electromagnetic wave attenuation. Fig. S1 shows a schematic diagram of the simulated cross-section, and Fig. S2 presents the initial complex permittivity and theoretical equivalent complex permittivity derived from previous exploratory studies.

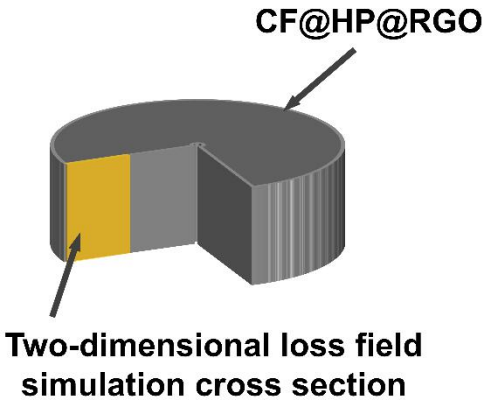

Figure S1 Schematic diagram of a two-dimensional axisymmetric model.

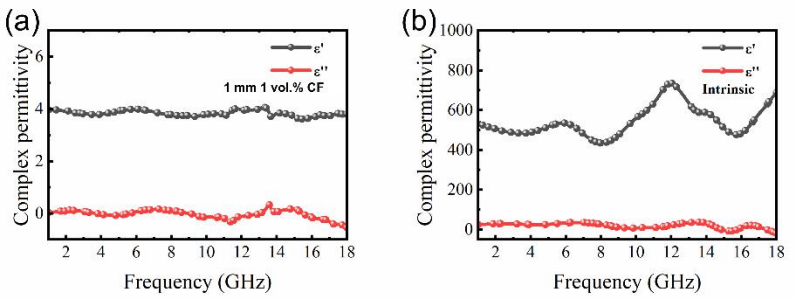

Figure S2 The complex permittivity of CF and (b) the intrinsic complex permittivity of CF.

Characterization:

The morphology and element mapping of samples were obtained by Scanning electron microscopy (SEM, ZEISS Merlin Compact, with an accelerated voltage of 20 kV). The lattice structure and electron diffraction pattern were observed on Transmission electron microscopy (TEM, Talos F200X). Powder X-ray diffraction (XRD, Empyrean with Cu-Ka radiation) was employed to determine the crystalline structure of all the samples across the range of 5 to 90◦ at a scanning step of 10◦/min. The stage information of elements and phase composition in all the samples was chartered by X-ray photoelectron spectroscopy (XPS, ESCALAB 250Xi). The functional groups of HPAA were characterized with Fourier transform infrared spectroscopy (FTIR, Nexus670, Nicolet) using a sample dispersed in KBr pellets in the wavenumber range of 500-4000 cm^{-1}. A Raman spectrometer (LabRam HR Evolution) was used to investigate the graphitization degree of carbon fiber. The contents of sp2 and sp3 carbon were calculated using the integral area based on the dual-window method. The results are as follows[5]:

$$sp^2 = \frac{A_G}{A_G + A_D} \times 100\% \quad (1)$$

Figures and Table

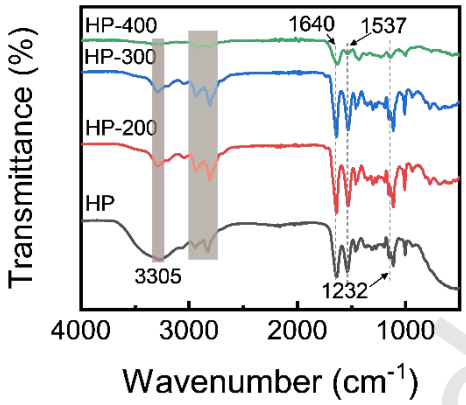

Figure S3. Fourier Transform Infrared Spectra of HP, HP-200, HP-300, and HP-400.

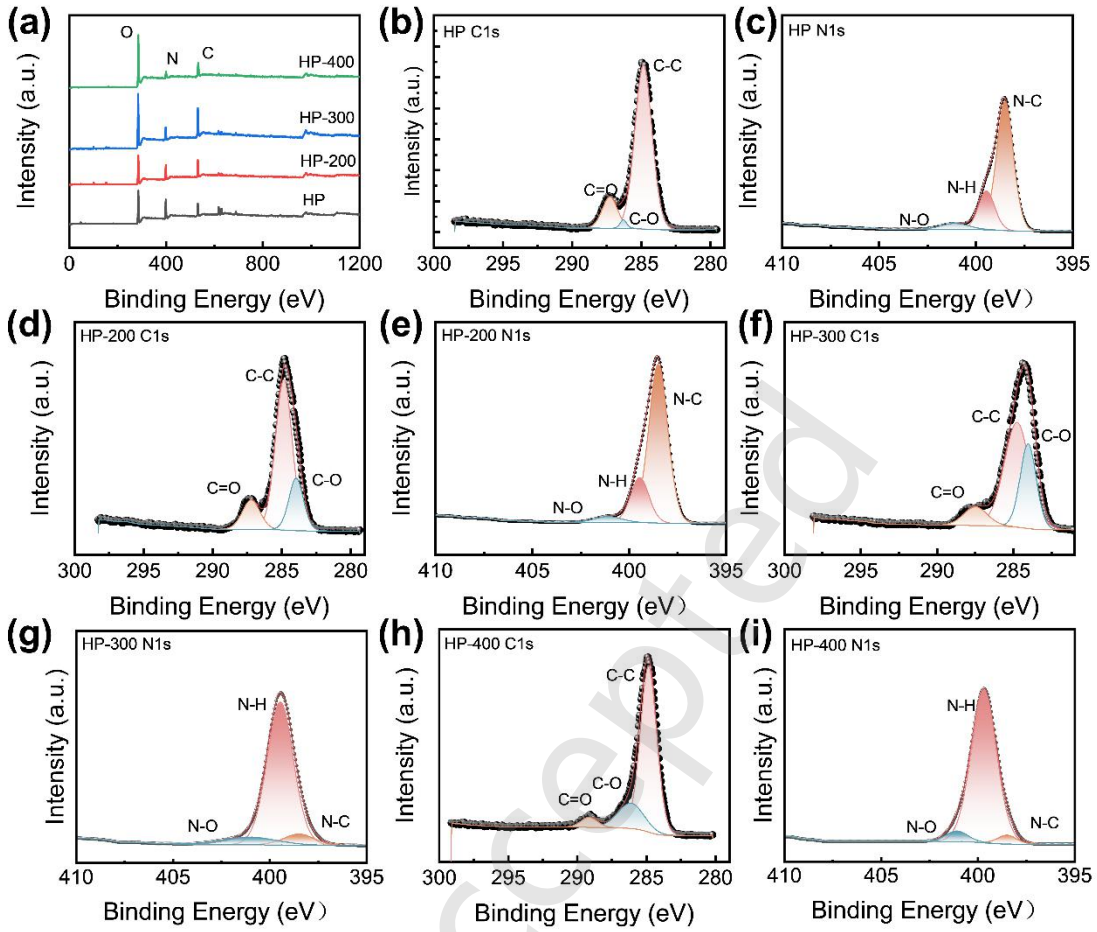

Figure S4. XPS spectra of HP~HP-400. (a) Overall XPS spectrum. HP XPS (b) C1s spectrum and (c) N1s spectrum. XPS of HP-200: (d) C1s spectrum and (e) N1s spectrum. XPS of HP-300: (f) C1s spectrum and (g) N1s spectrum. XPS of HP-400: (h) C1s spectrum and (i) N1s spectrum.

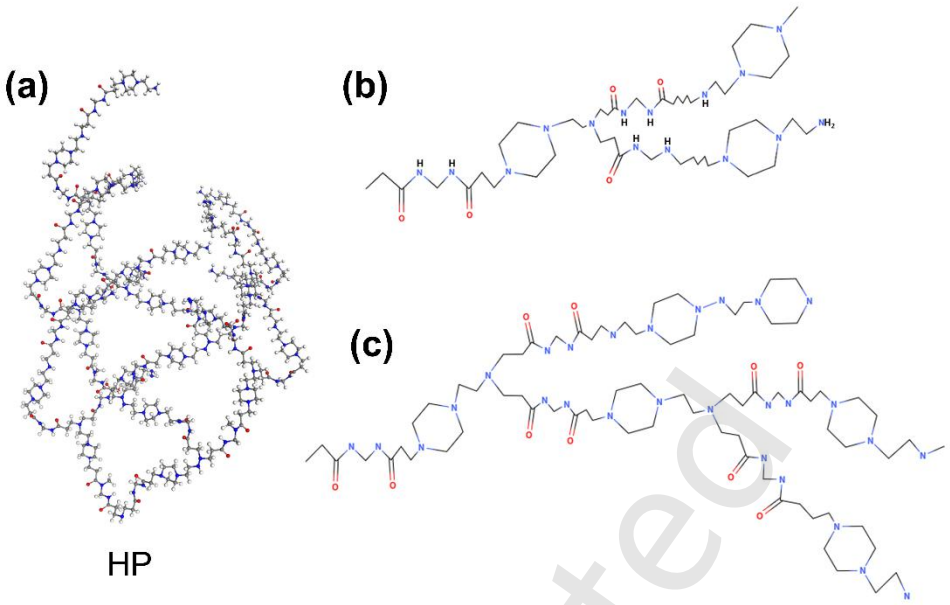

Figure S5. Schematic diagram of HP polymer structure. (a) Molecular structure schematic. (b, c) Schematic diagrams of different branched structures (showing that most typical bonds involve N-H, C-N, and C=O interactions).

Figure S6 HP optical images after thermal reduction.

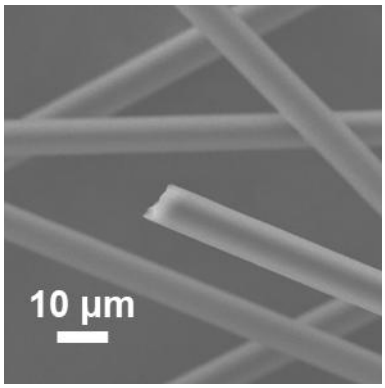

Figure S7 SEM of CF.

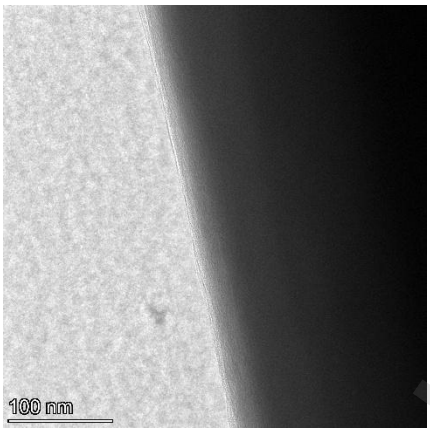

Figure S8. The TEM of CF.

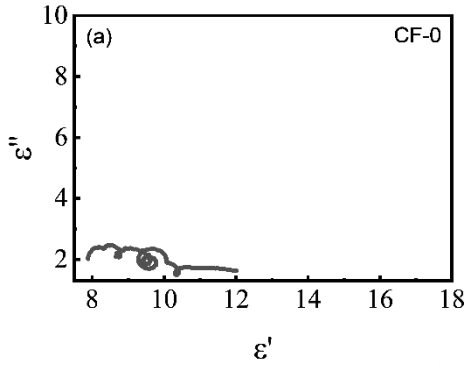

Figure S9. The Cole-Cole of CF-0.

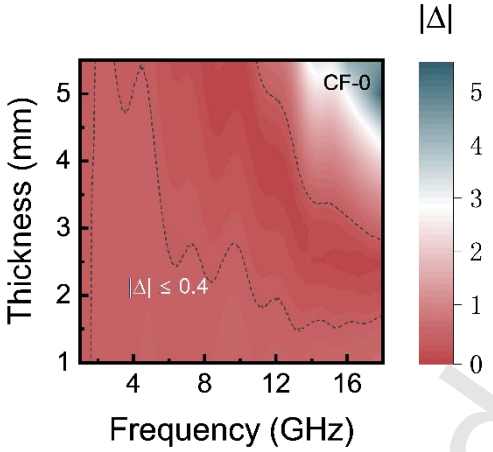

Figure S10. The |△| of CF-0.

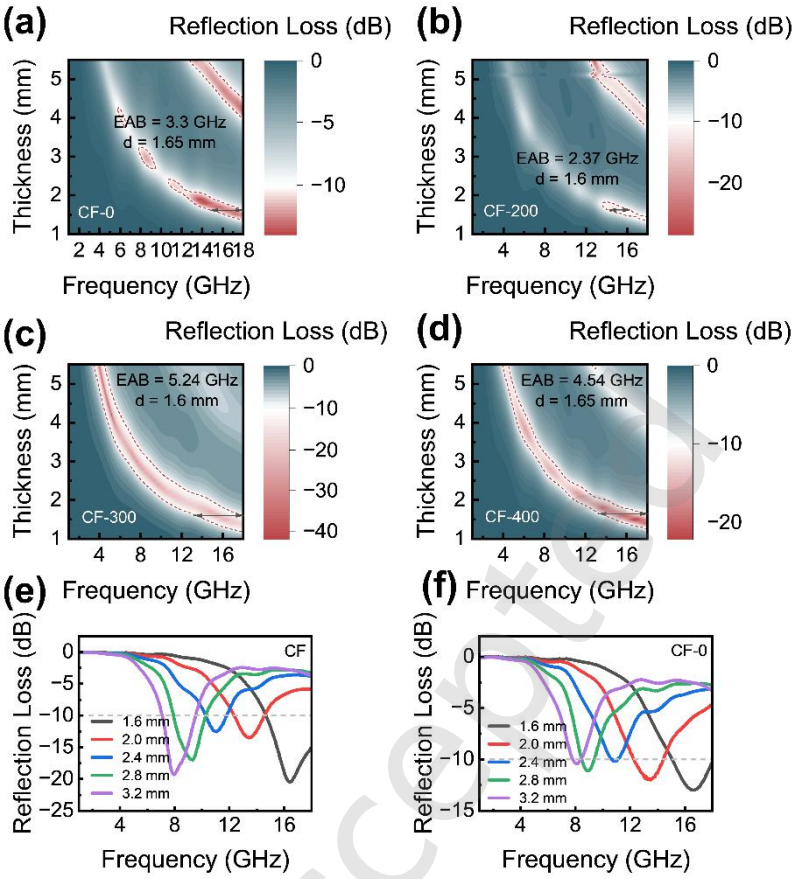

Figure S11 (a) CF-0, (b) CF-200, (c) CF-300, and (d) CF-400 reflectance loss distribution two-dimensional diagrams. (e) CF and (f) CF-0 reflectance loss curves.

Table S1

Material	SEAB	SRL	
$Co_3SnC_{0.7}$ nanoparticles	0.59	4.45	[29]
Ni/MnO-carbon aerogel	0.27	2.37	[30]
CNT/cellulose aerogel	0.27	2.04	[31]
Sugarcane carbon aerogel	0.23	1.79	[32]
PIC/rGO porous carbon	0.11	0.97	[33]
Kevlar/CNT aerogel fiber	0.27	2.73	[34]
α-FeOOH/carbon aerogel	0.2	1.27	[35]
CoNiO/rGO aerogel	0.75	4.21	[36]
FeCo@CCA aerogel	0.71	4.78	[37]
$CoFe_2O_4$ /AC composite	0.12	1.98	[38]
CNT carbon fiber absorber	0.28	1.59	[39]
biomass porous carbon	0.19	1.48	[40]
MOF-derived carbon	0.19	1.54	[41]
graphene aerogel	0.11	0.95	[42]
CF@HP@RGO	0.64	5.15	This work

Reference

[1] Gao J, Liu C, Miao L, Wang X, Chen Y. Free-Standing Reduced Graphene Oxide Paper with High Electrical Conductivity. Journal of Electronic Materials. 2016;45(3):1290-5.
[2] Ramamoorthy H, Buapan K, Chiawchan T, Thamkrongart K, Somphonsane R. Exploration of the temperature-dependent correlations present in the structural, morphological and electrical properties of thermally reduced free-standing graphene oxide papers. Journal of Materials Science. 2021;56(27):15134-50.
[3] Botcha VD, Narayanam PK. Green and solid state reduction of GO monolayers sandwiched between Arachidic acid LB layers. Diamond and Related Materials. 2024;148:111506.
[4] Seon Lee Y, Ryeol Kim N, Ki Park S, Ko Y-i, Shin Y, Yang B, et al. Effects of high-temperature thermal reduction on thermal conductivity of reduced graphene oxide polymer composites. Applied Surface Science. 2024;650:159140.
[5] Zhang C, Jiang J-T, Guan Z, Zhang Y, Li Y, Song B, et al. Unveiling the sp2-sp3 C-C Polar Bond Induced Electromagnetic Responding Behaviors by a 2D N-doped Carbon Nanosheet Absorber. ADVANCED SCIENCE. 2024;11(4).